

Supporting Information

for

Optochemically Responsive 2D Nanosheets of a 3D Metal-Organic Framework Material

Abhijeet K. Chaudhari,¹ Ha Jin Kim,² Intaek Han,² and Jin-Chong Tan^{1}*

*¹Department of Engineering Science, University of Oxford, OX1 3PJ, Oxford,
United Kingdom*

*²Samsung Advanced Institute of Technology (SAIT), Samsung Electronics Co. Ltd.,
South Korea*

*Correspondence to: jin-chong.tan@eng.ox.ac.uk

Table of Contents

1	Materials and Methods.....	3
1.1	Synthesis of Porous OX-1 2D Nanosheets as Host Framework Material.....	3
1.2	Synthesis of Functionalized MOF Nanosheets: ZnQ _{DMF} @OX-1 and ZnQ _{DMA} @OX-1.....	4
2	SEM Images of Supramolecular Gels and Exfoliated Nanosheets	7
3	TEM Images of Supramolecular Gels and Exfoliated 2D MOF Nanosheets	9
4	AFM Topography Images of OX-1 Nanosheets	14
5	Nanosheet Thickness Characterization	15
6	Powder X-Ray Diffraction (PXRD) to Determine Crystal Structure of the OX-1 MOF Nanosheets	18
7	Thermogravimetric Analysis (TGA).....	22
8	Raman Spectroscopy.....	24
9	Quantum Yield and Lifetime of Pristine and Functionalized OX-1 Nanosheets.....	25
10	Geometry Optimization and Band Gap Calculations.....	26
11	Host-Guest Interaction and Optochemical Stimulation	37
12	References.....	40

1 Materials and Methods

1.1 Synthesis of Porous OX-1 2D Nanosheets as Host Framework Material

2 mL *N,N*-Dimethylformamide (DMF) clear solution of $\text{Zn}(\text{NO}_3)_2$ (1.5 mmol, termed Solution A) was combined with 3 mL clear solution of 1,4-Benzenedicarboxylic acid (3 mmol, BDC) plus Triethylamine (NEt_3^+) (6 mmol) (termed Solution B). We found fibrous hybrid materials formed immediately upon combining solutions A and B.

The hybrid fiber material containing nanosheets was washed with copious amounts of DMF, methanol and acetone to break down the gel fibres, thereby releasing pure nanosheets of porous MOF material: $(\text{HNEt}_3)_2[\text{Zn}_3\text{BDC}_4]\cdot\text{DMF}$ (we designate as “OX-1” MOF nanosheets). Further sonication step can be used to exfoliate the OX-1 material into even thinner 2D sheets, which suggests the presence of weak molecular interactions between the adjacent 3D MOF structure hence permitting facile 2D exfoliation. Finally, the nanosheets harvested were separated by centrifugation (8000 rpm) and then subjected to vacuum drying at 110 °C for 4 hours.

1.2 Synthesis of Functionalized MOF Nanosheets: $\text{ZnQ}_{\text{DMF}}@OX-1$ and $\text{ZnQ}_{\text{DMA}}@OX-1$

Preparation of functionalized MOF nanosheet materials ($\text{Guest}@OX-1$) involves a simple additional step of *in situ* mixing of *N,N*-Dimethylformamide (as clear solution) containing guest species *e.g.* ZnQ/AlQ/Naphthalene/Anthracene/Fluorescein into Solution B (see §1.1). This facile high-concentration reaction (HCR) method is shown below.

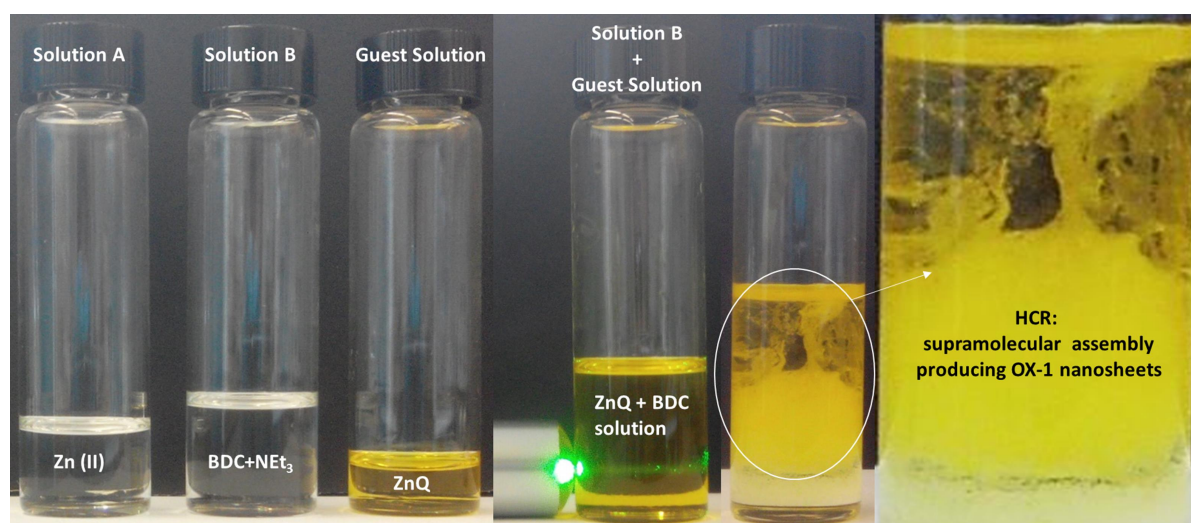


Figure shows clear solutions of Zn(II) in DMF (Solution A), BDC linker plus NEt_3^+ in DMF (Solution B), and ZnQ guest solution. Image on the far right shows the high-concentration reaction (HCR) when combining the A + B + ZnQ guest solutions, producing *instantaneous* supramolecular assembly containing OX-1 nanosheet materials.

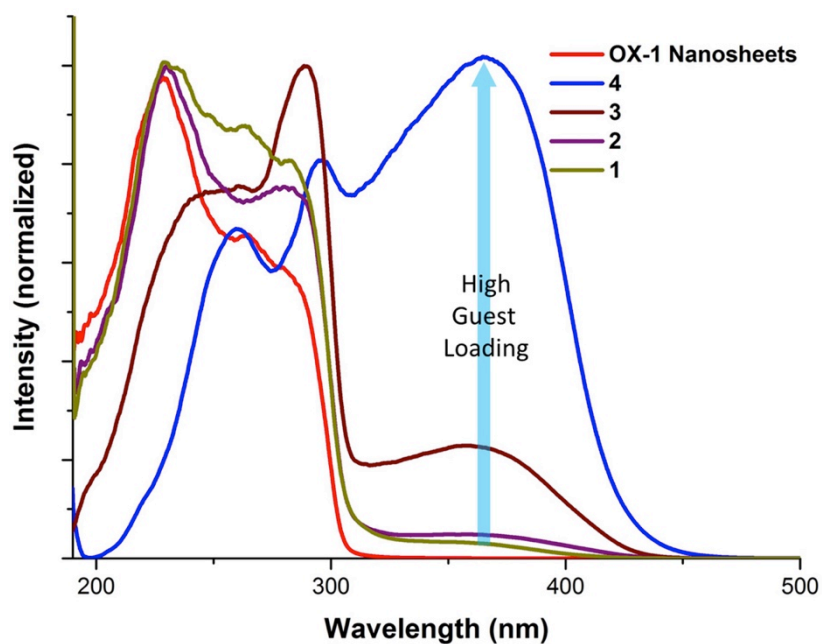
To ensure that luminescent guests are not left adhered to the MOF surface, we have washed the product thoroughly twice using solvents that will solubilise the guest species (first using DMF, followed by methanol and acetone). Note that the washing step is carried out with simultaneous sonication (10 minutes per solvent, then centrifugation) to further expedite the removal of external guest species. Mixture of solvents (Benzene: *N,N*-Dimethylformamide = 1:2) was used for Anthracene or Naphthalene guest solution, and the same solvent mixture was used for washing the product material to remove excess reactants.

We prepared the different “guest solutions” in accordance to the following steps:

- a) **ZnQ**: ZnQ was synthesized in 1 mL of *N,N*-Dimethylformamide by reacting 1:2 molar ratio of Zn(II), (0.5 mmol) and 8-Hydroxyquinoline (8HQ), (1.0 mmol).
- b) **AlQ**: AlQ was synthesized in a similar manner to that of ZnQ except by taking 1:3 molar ratio of Al(III), (0.5 mmol) and 8HQ (1.5 mmol).
- c) **Naphthalene**: 0.5 mmol of Naphthalene was dissolved in 1.5 mL of Benzene and then it was mixed with 1.5 mmol solution of Zn(II) in 3 mL of *N,N*-Dimethylformamide prior to the reaction with BDC linker solution.
- d) **Anthracene**: 0.5 mmol of Anthracene was dissolved in 2 mL of Benzene and then mixed with Zn(II) solution in 3mL of *N,N*-Dimethylformamide and sonicated further to prepare a clear solution.
- e) **Fluorescein**: 0.1 mmol of Fluorescein was dissolved in 1 mL of DMF and mixed with Zn(II) solution before reaction with the BDC linker.

Furthermore, we have performed a systematic set of reactions to show that it is possible to control the loading of guest species confined within the OX-1 nanosheet host framework. Changes in the absorption behavior of the different products as a function of guest loading are plotted in figure below.

Reaction #	ZnQ (Guest Concentration)		Zn-BDC (OX-1 Concentration)	
	Zn(II)	8HQ	Zn(II)	BDC ²⁻
1	0.1 mmol	0.2 mmol	1.5 mmol	3.0 mmol
2	0.3 mmol	0.6 mmol	1.5 mmol	3.0 mmol
3	0.5 mmol	1.0 mmol	1.5 mmol	3.0 mmol
4	1.0 mmol	2.0 mmol	1.5 mmol	3.0 mmol



Controlled experiment with loading of various amounts of ZnQ guest emitters in OX-1 nanosheet host material (table above). Notice how the absorption spectra being modified significantly with higher guest concentration loading, signifying a stronger host-guest coupling effect.

2 SEM Images of Supramolecular Gels and Exfoliated Nanosheets

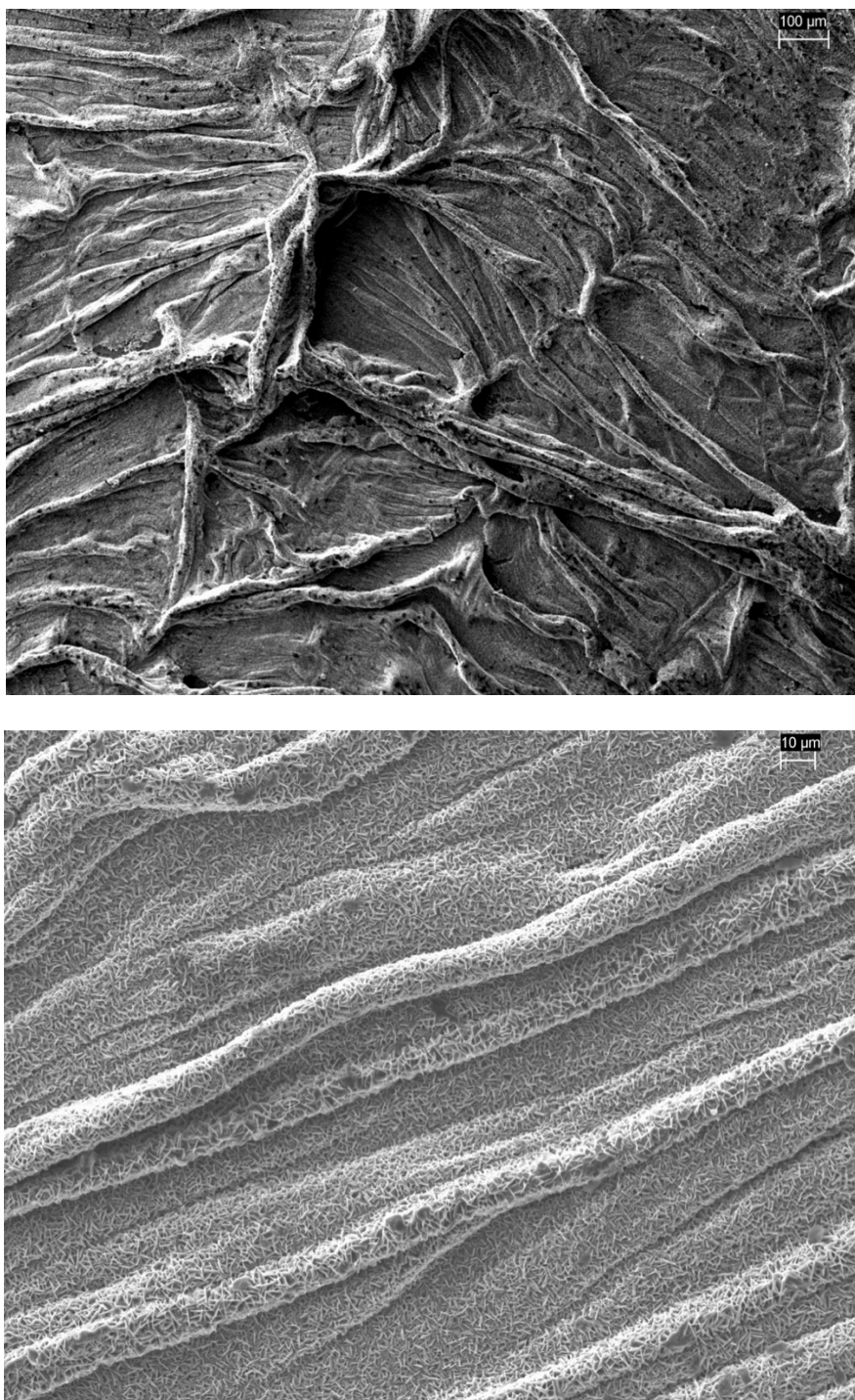


Figure S1. SEM images of fibrous supramolecular materials derived from high concentration reaction (HCR), obtained by layering of reactant solutions onto a glass substrate.

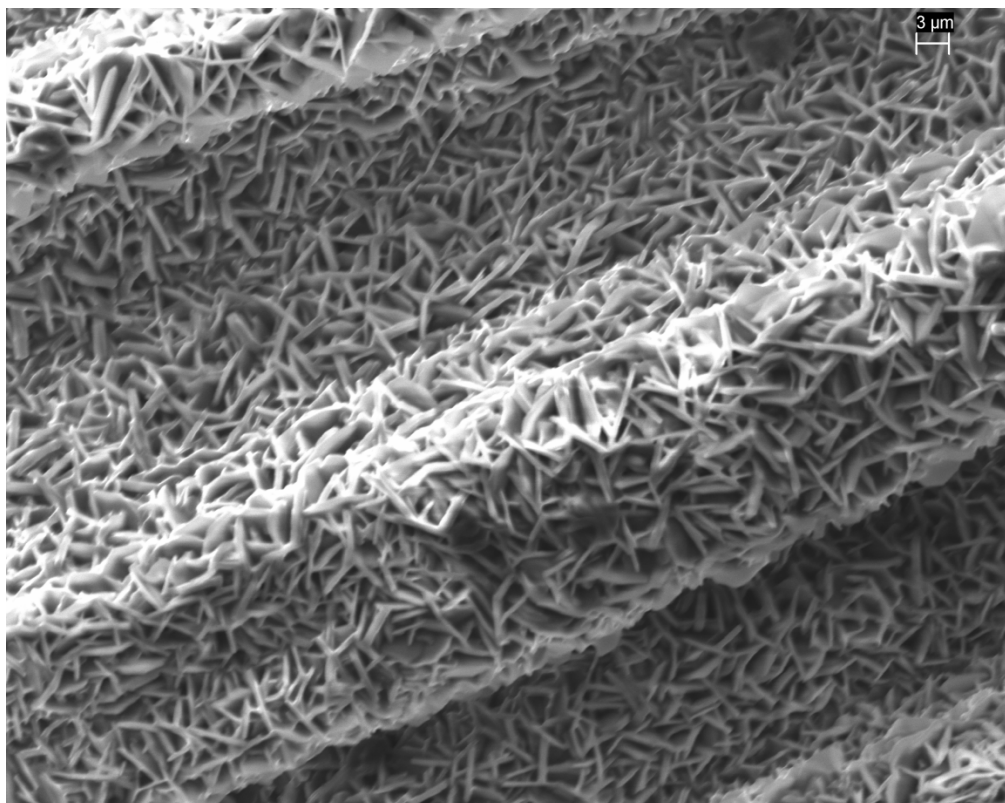


Figure S2. Enlarged SEM image showing densely grown 2D nanosheet structures generated through fibrous hybrid assembly at room temperature, enabled by rapid HCR approach.

3 TEM Images of Supramolecular Gels and Exfoliated 2D MOF Nanosheets

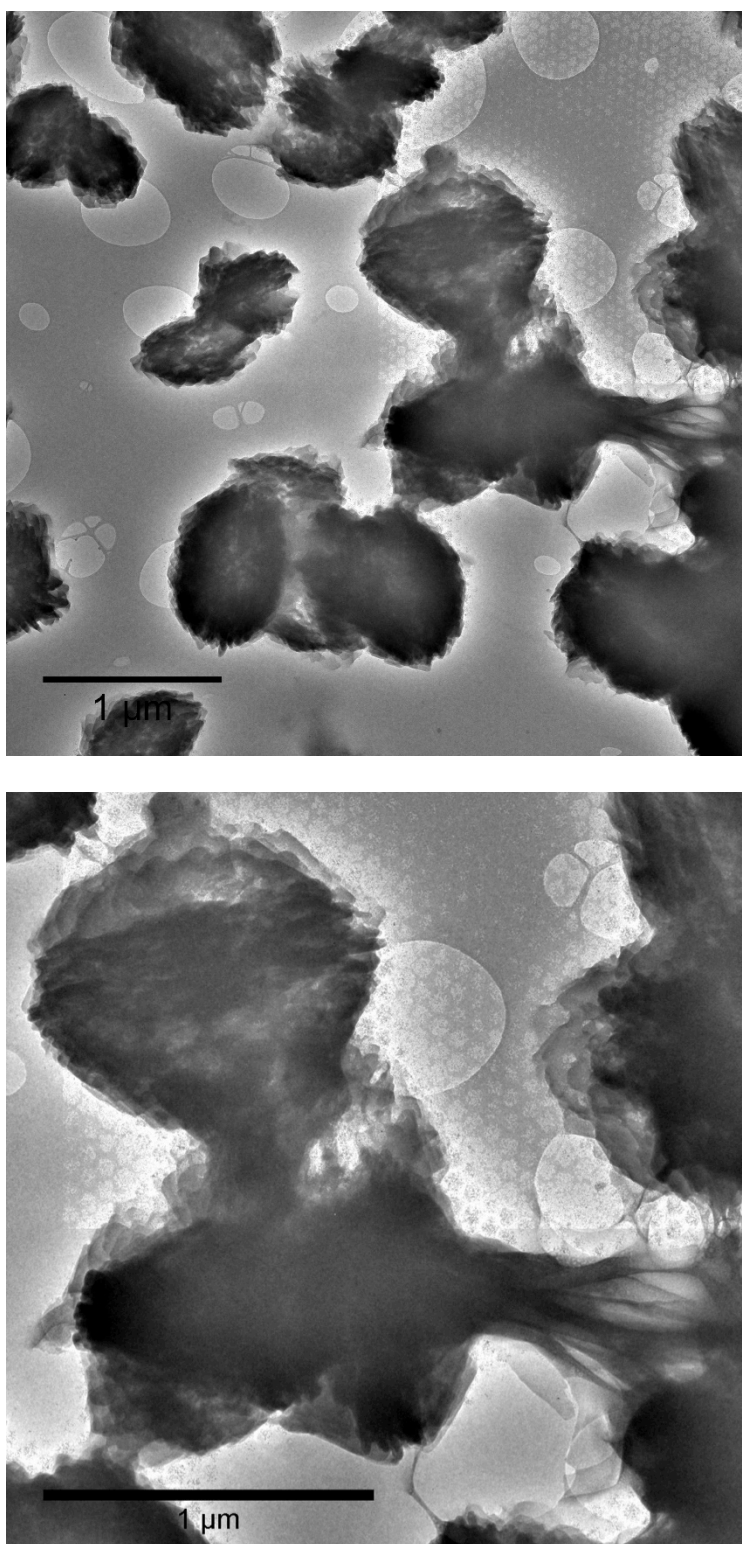


Figure S3. TEM image showing large clusters of 2D nanosheets embedded in a partially disintegrated supramolecular gel network. Samples are supported on a TEM grid (holey carbon background visible).

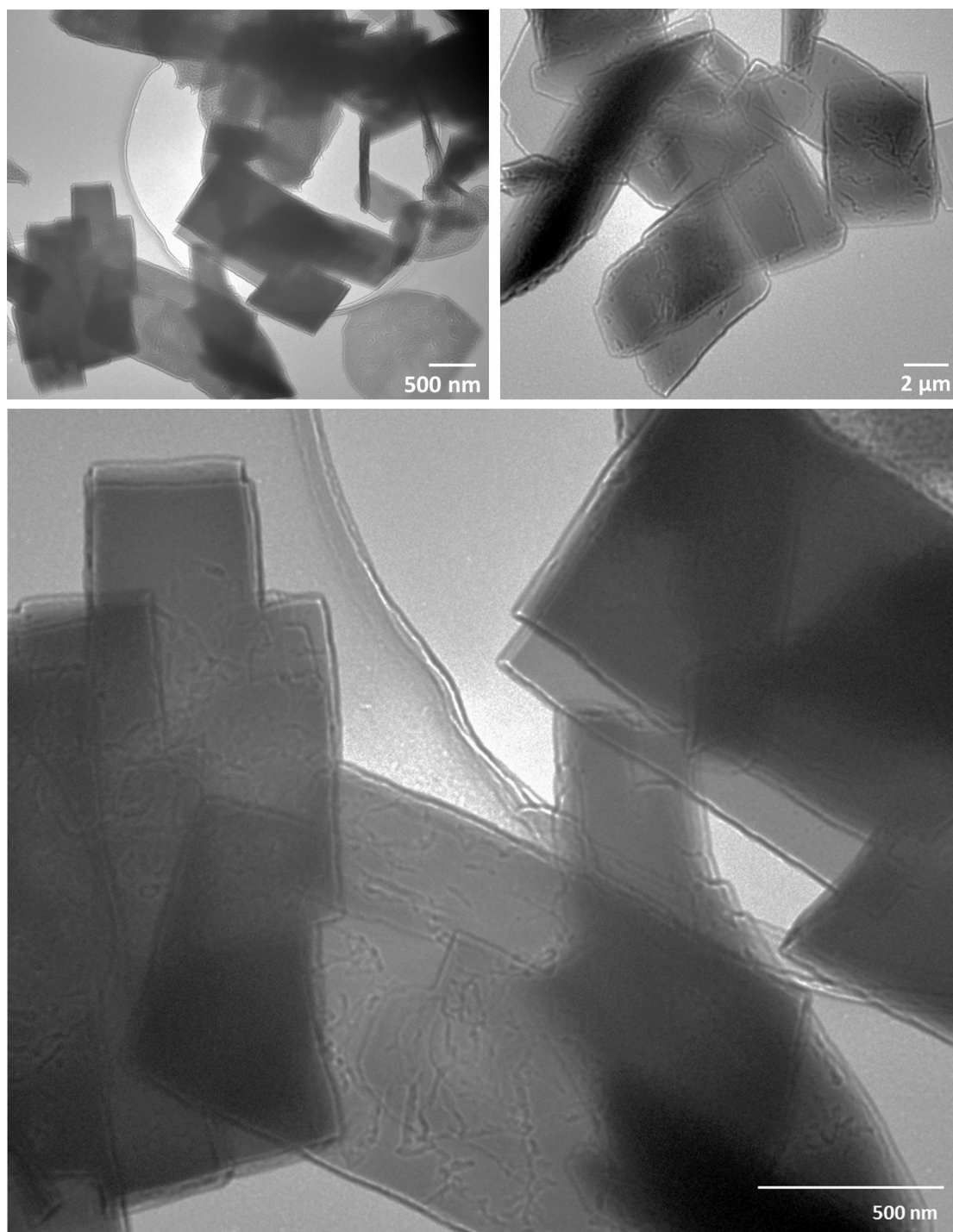


Figure S4. TEM showing nanosheet structures of a pristine OX-1 material revealing well defined rectangular 2D thin-sheet morphology.

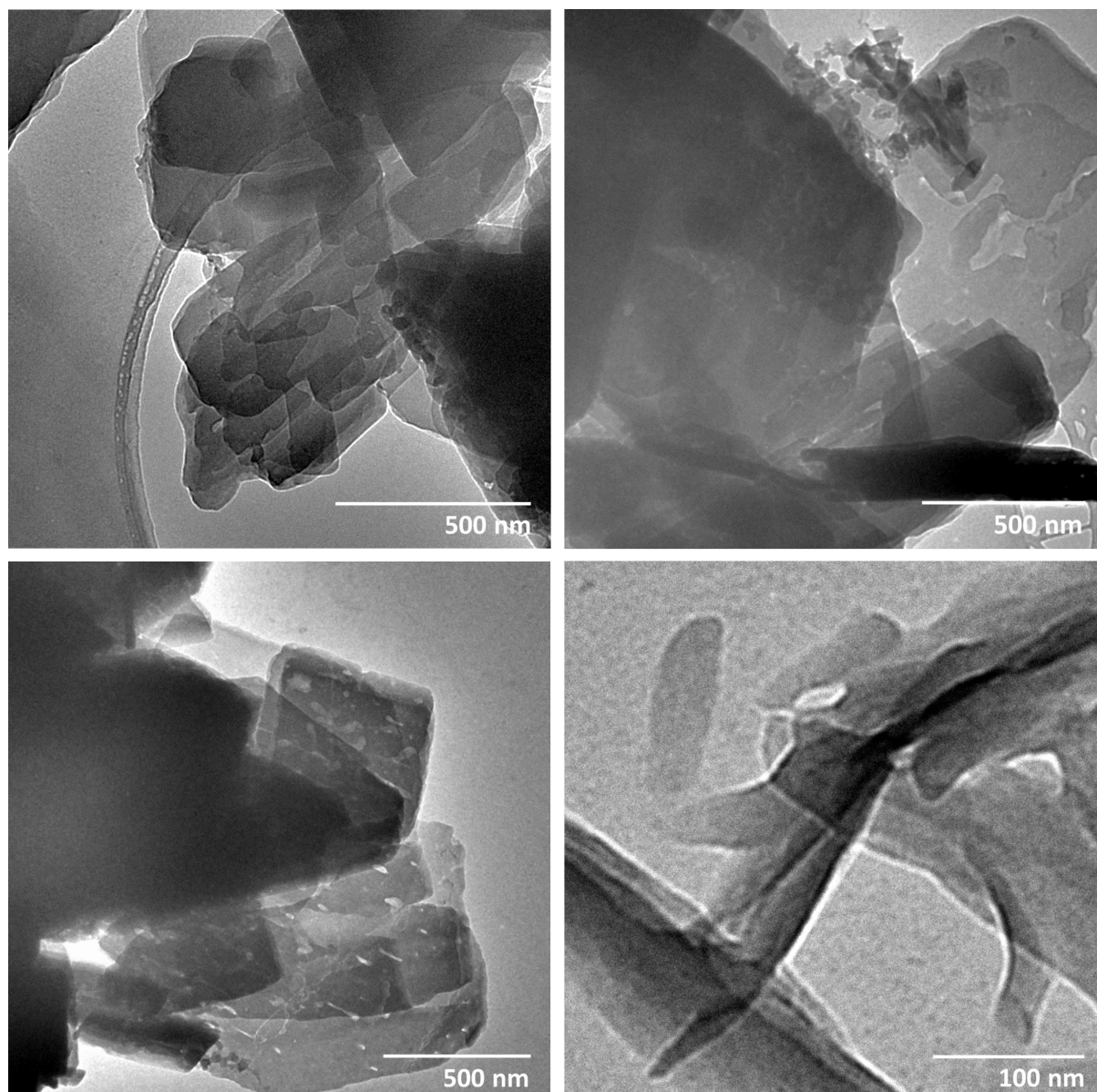


Figure S5. TEM micrographs of OX-1 nanosheets synthesized in DMA solvent, revealing thin 2D sheet morphology.

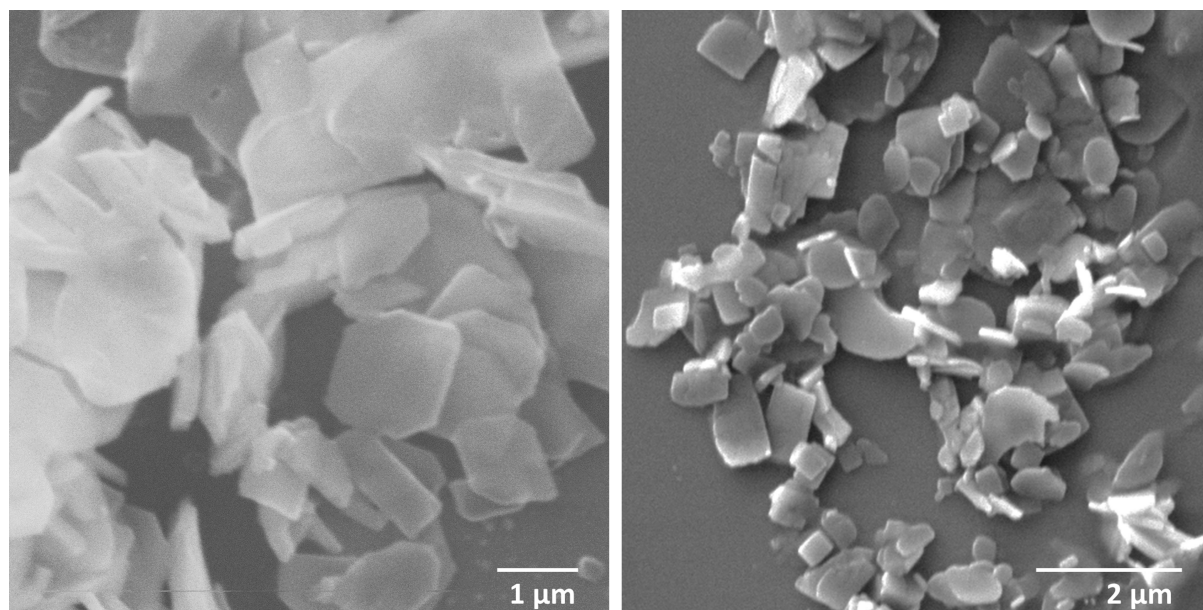


Figure S6. SEM micrographs of OX-1 nanosheets synthesized in DMA solvent.

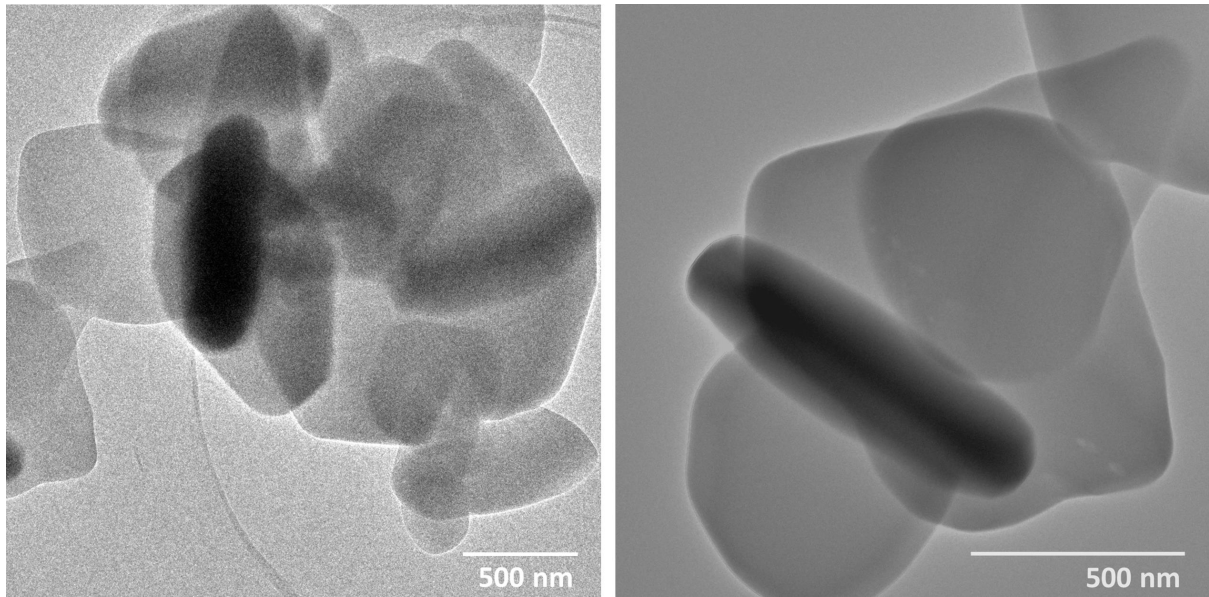


Figure S7. TEM micrographs of ZnQDMA@OX-1 nanosheets.

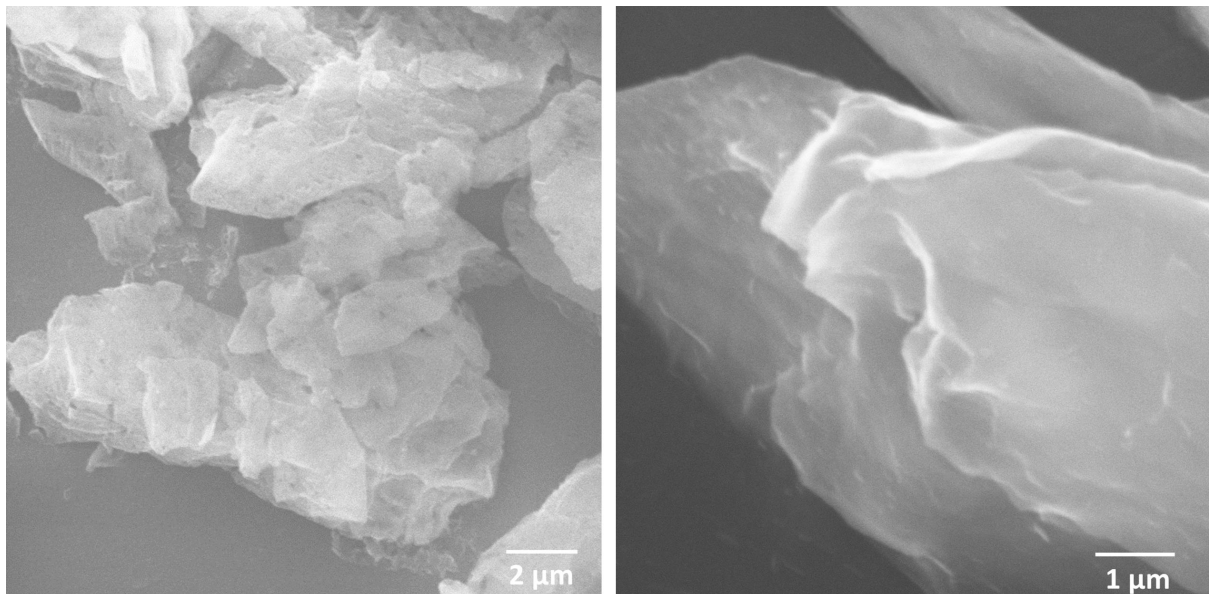


Figure S8. SEM micrographs of ZnQDMA@OX-1 nanosheets revealing thin two-dimensional morphologies.

4 AFM Topography Images of OX-1 Nanosheets

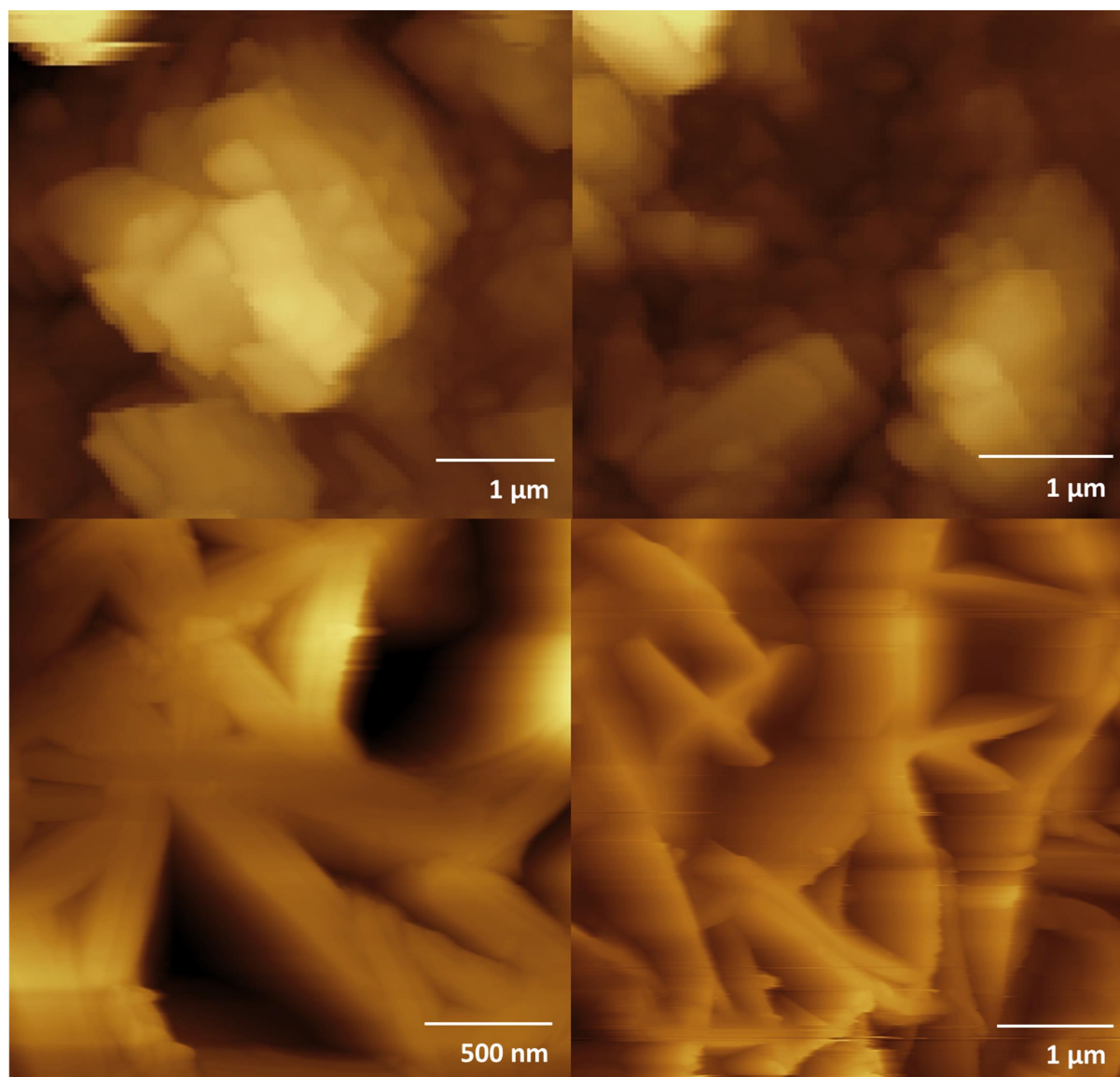


Figure S9. AFM showing 2D nanosheet structures and exfoliated layered morphologies of the OX-1 material.

5 Nanosheet Thickness Characterization

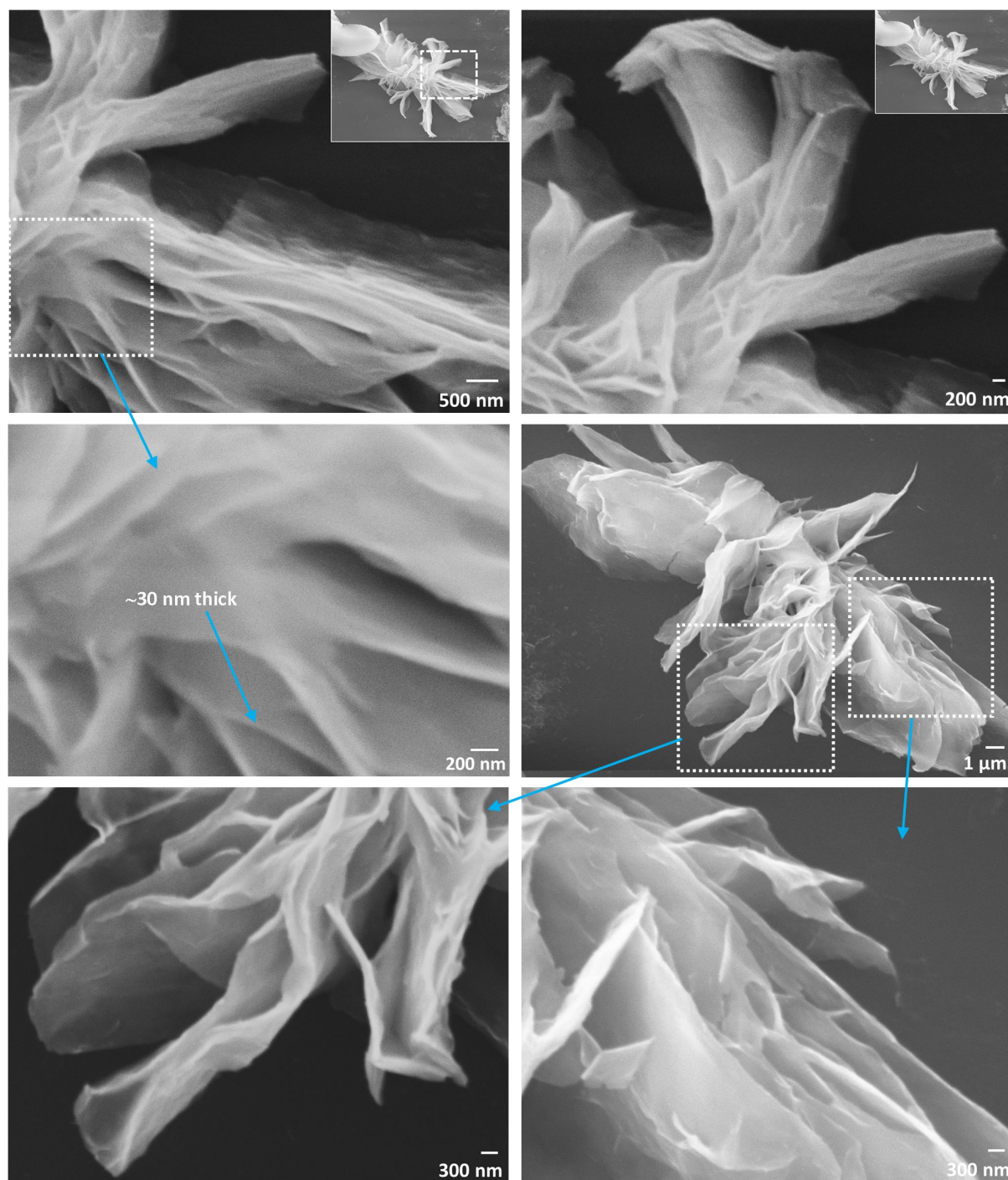


Figure S10. SEM imaging on functionalized nanosheet material i.e. $\text{ZnQ}_{\text{DMF}}@\text{OX-1}$ which clearly shows growth of thin extended sheets intertwined with each other as a result of high concentration reaction (HCR) approach. Layered $\text{ZnQ}_{\text{DMF}}@\text{OX-1}$ material started to delaminate after thorough washing and 1 hr sonication. These images also give insights into how multiple layers of nanosheets are stacked together prior to the exfoliation step.

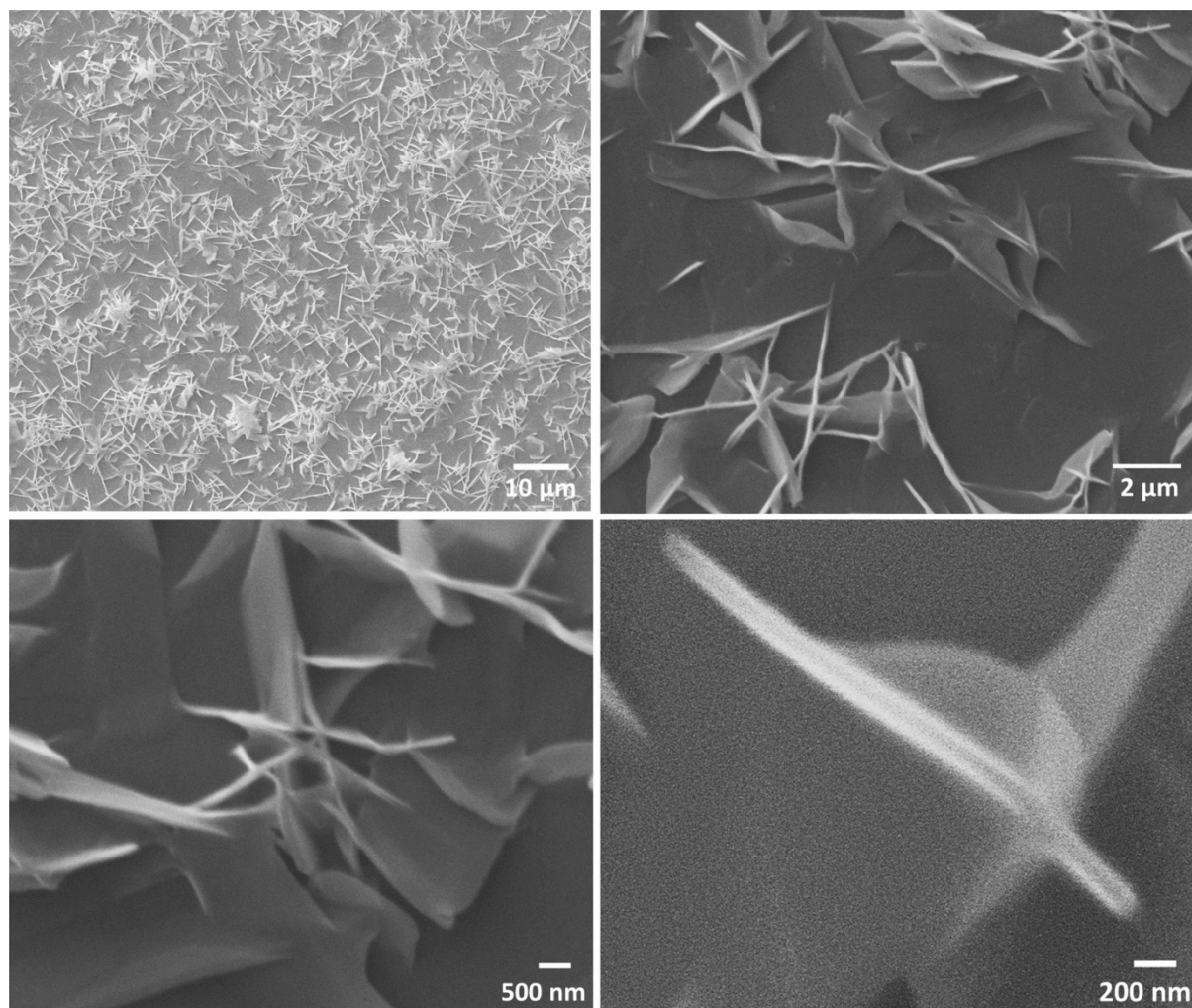


Figure S11. SEM of a thoroughly washed pristine OX-1 MOF material after 1 hr sonication. Prevalence of thin foils confirms facile exfoliation of OX-1 into 2D nanosheets.

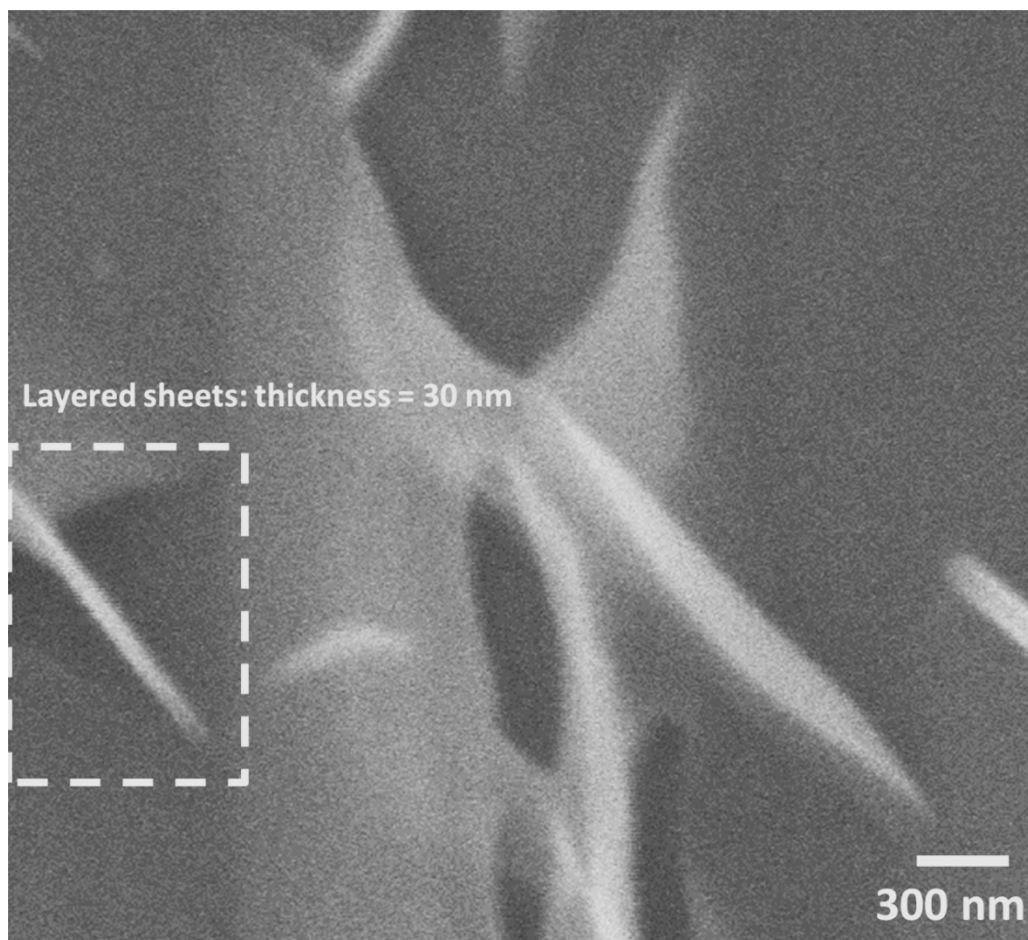


Figure S12. SEM of OX-1 nanosheet structures, revealing a thickness of ~30 nm of an exfoliated MOF layer.

6 Powder X-Ray Diffraction (PXRD) to Determine Crystal Structure of the OX-1 MOF Nanosheets

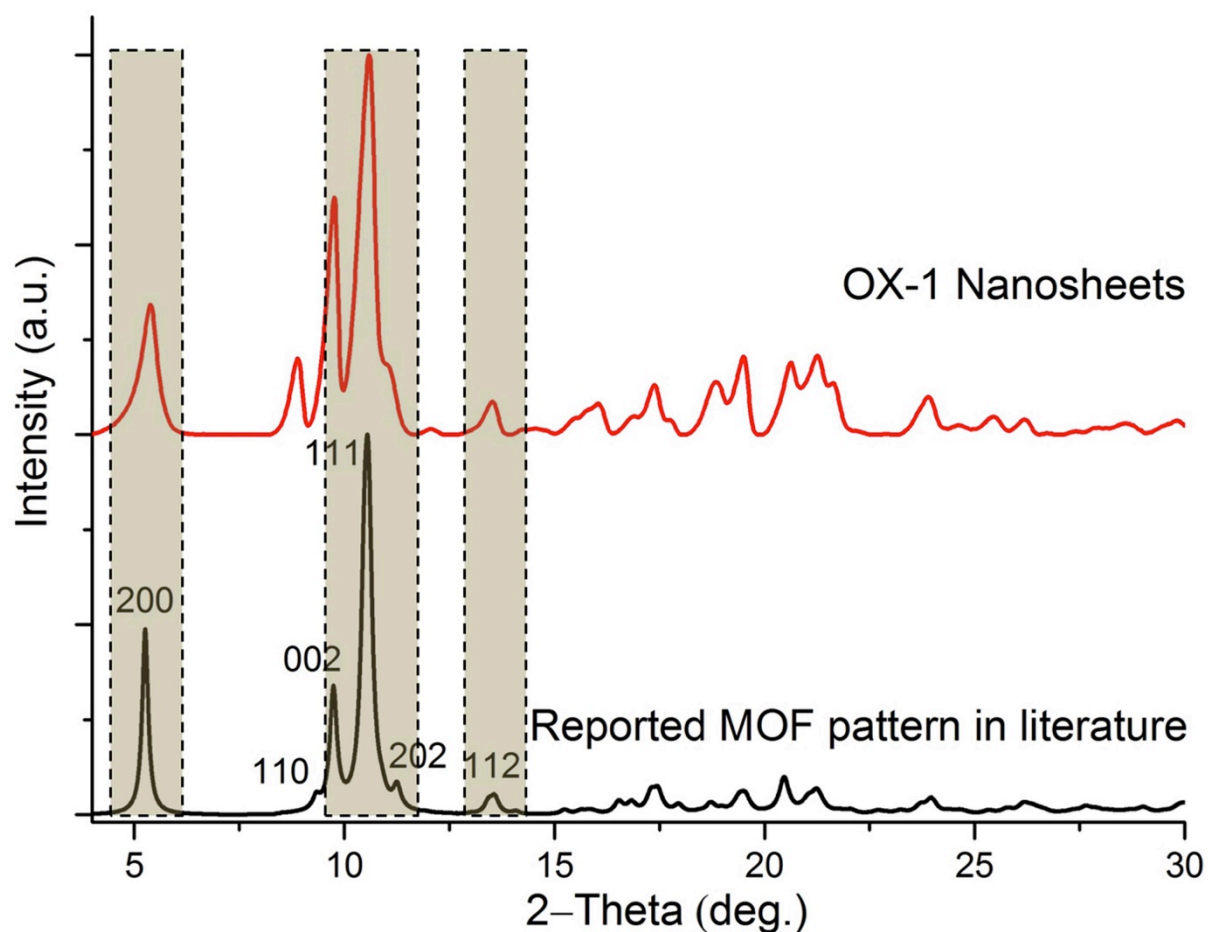


Figure S13. Comparison between (simulated) X-ray diffraction pattern of reported 3D MOF structure [1,2] and that of the 2D nanosheet structure experimentally obtained in current work. The detected changes in PXRD pattern are linked to lattice distortion caused by charge balancing NEt_3^+ cations occupying the OX-1 MOF pores. Peak broadening is associated with the nanoscale morphology of the layered OX-1 nanosheets (see TEM and SEM images).

Table S1. Structural parameters determined by Pawley refinement of the X-ray diffraction data (performed in Reflex module in Accelrys Material Studio v.8), compared with reported MOF structures with a higher symmetry.

Compound	OX-1 Nanosheets	MOF reported by Burrows <i>et al</i> [1]	MOF reported by Stock <i>et al</i> [2]
Crystal System	Triclinic	Monoclinic	Monoclinic
Space Group	P1	C2/c	C2/c
X-ray Source	CuK α	not mentioned	MoK α
λ [Å]	1.5418	-	0.71073
Refined Range [°]	4 to 40	-	-
a [Å]	33.576	33.6075	33.3724
b [Å]	9.8147	9.8727	9.8317
c [Å]	18.2668	18.1642	18.1967
α [°]	90.1257	90.00	90.00
β [°]	90.5996	92.226	92.4550
γ [°]	90.4146	90.00	90.00
Volume [Å ³]	6019.11	6022.27	5964.99
Step Size	0.02	-	-
Peak Profile	Pseudo-Voigt	-	-
R factors	0.084 (R _{wp}) 0.09 (R _p)	0.0510 (R1) 0.1458 (wR2)	0.0395 (R1) 0.0843 (wR2)

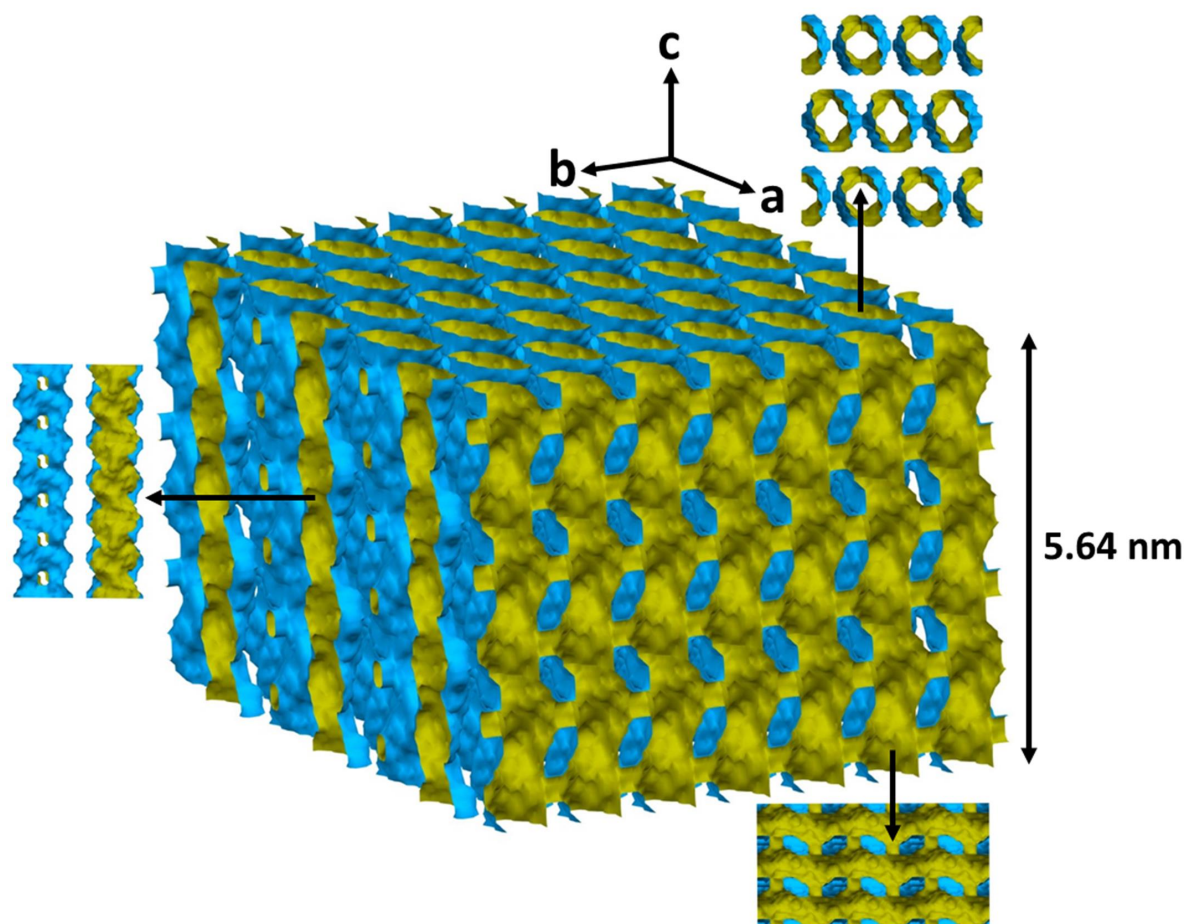


Figure S14. Molecular packing diagram of OX-1 MOF material showing its solvent accessible volume (SAV), which are voids that can be infiltrated by guest molecules or to be occupied by specific analytes. Undulating 1D porous channels, whose diameter is ~ 1 nm, are running along the c -axis (shown here vertically). Void volume estimated using Mercury CSD[3] was found to be 34.3% corresponding to 2062.72 \AA^3 of empty void space per unit cell.

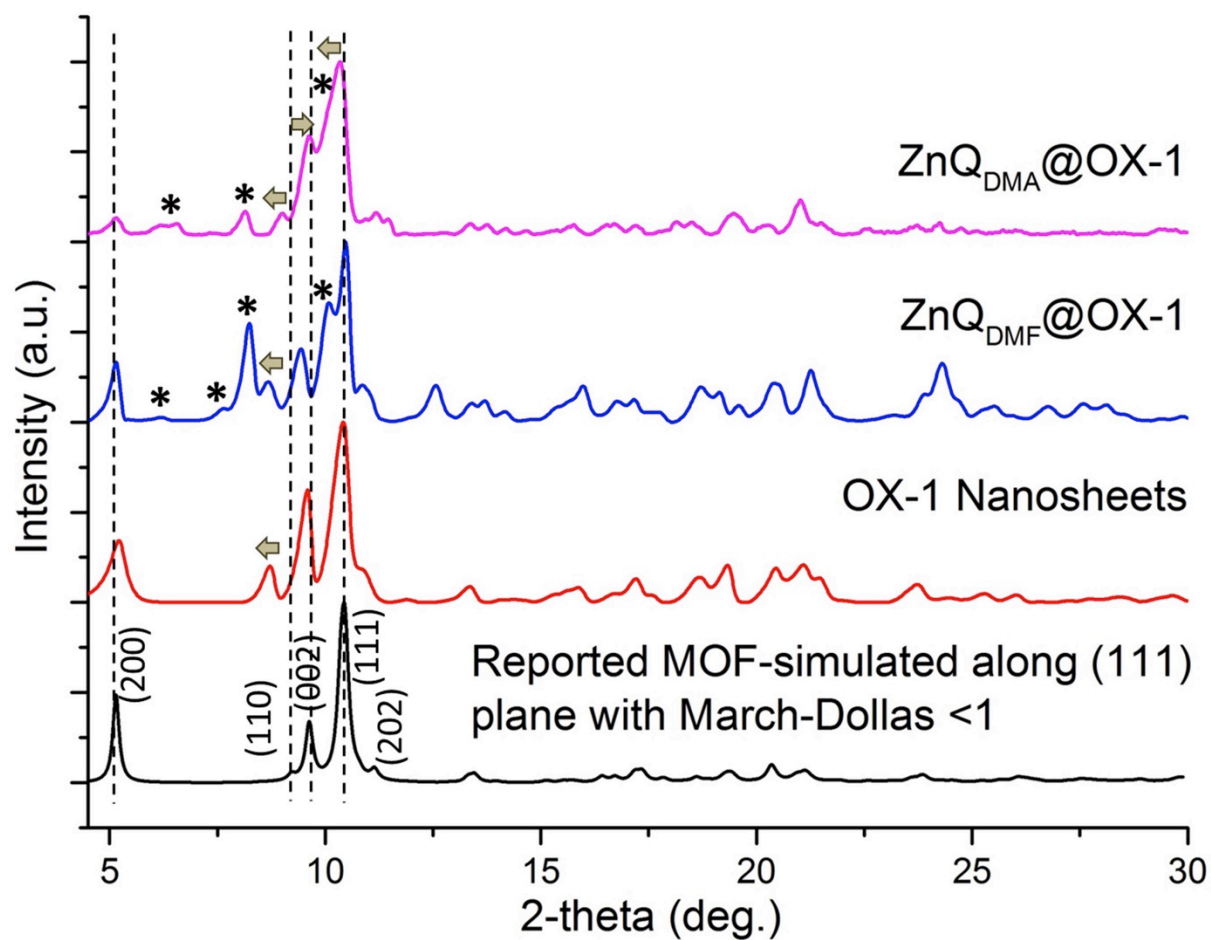


Figure S15. XRD patterns of MOF nanosheets with and without emissive ZnQ functional guests. Extra peaks are ascribed to the diffraction of ZnQ guest designated by the * symbol. Peak shift in OX-1 host in the case of ZnQ_{DMA}@OX-1 (marked by arrows on top of each peak at small angles) implies guest@host structural modification causing slight expansion in the cell dimensions.

7 Thermogravimetric Analysis (TGA)

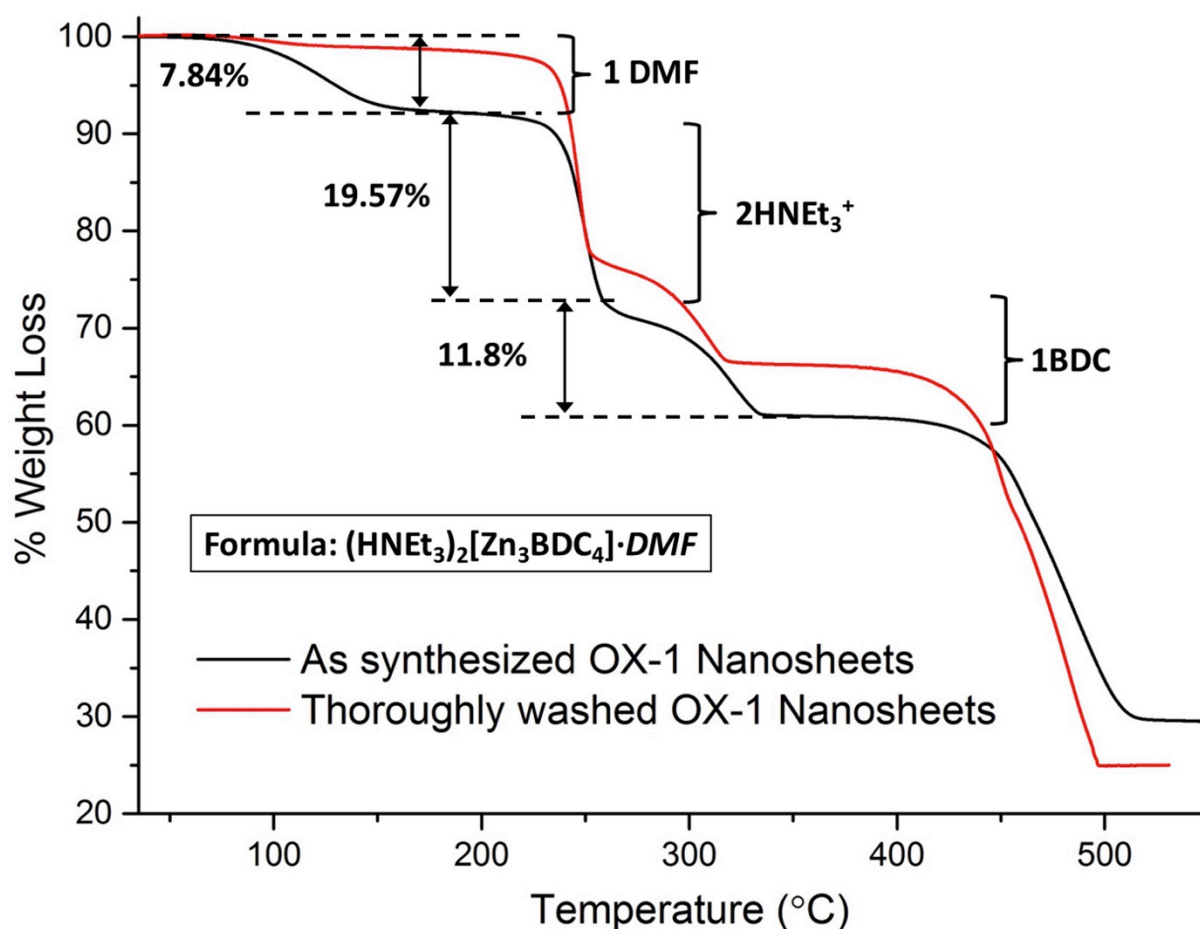


Figure S16. Thermogravimetric analysis (TGA) for OX-1·DMF nanosheet material synthesized in N,N-Dimethylformamide (DMF) revealing the formula for the material which is in close agreement to the expected weight loss of the components present in the material. Free solvent species occluded in the voids can be easily removed by thorough washing by low-boiling point solvent like Acetone and evacuated by heating and vacuum treatment. This behaviour is very similar to the reported MOF structure [1] where they claimed removal of BDC linker achieved in respective temperature range.

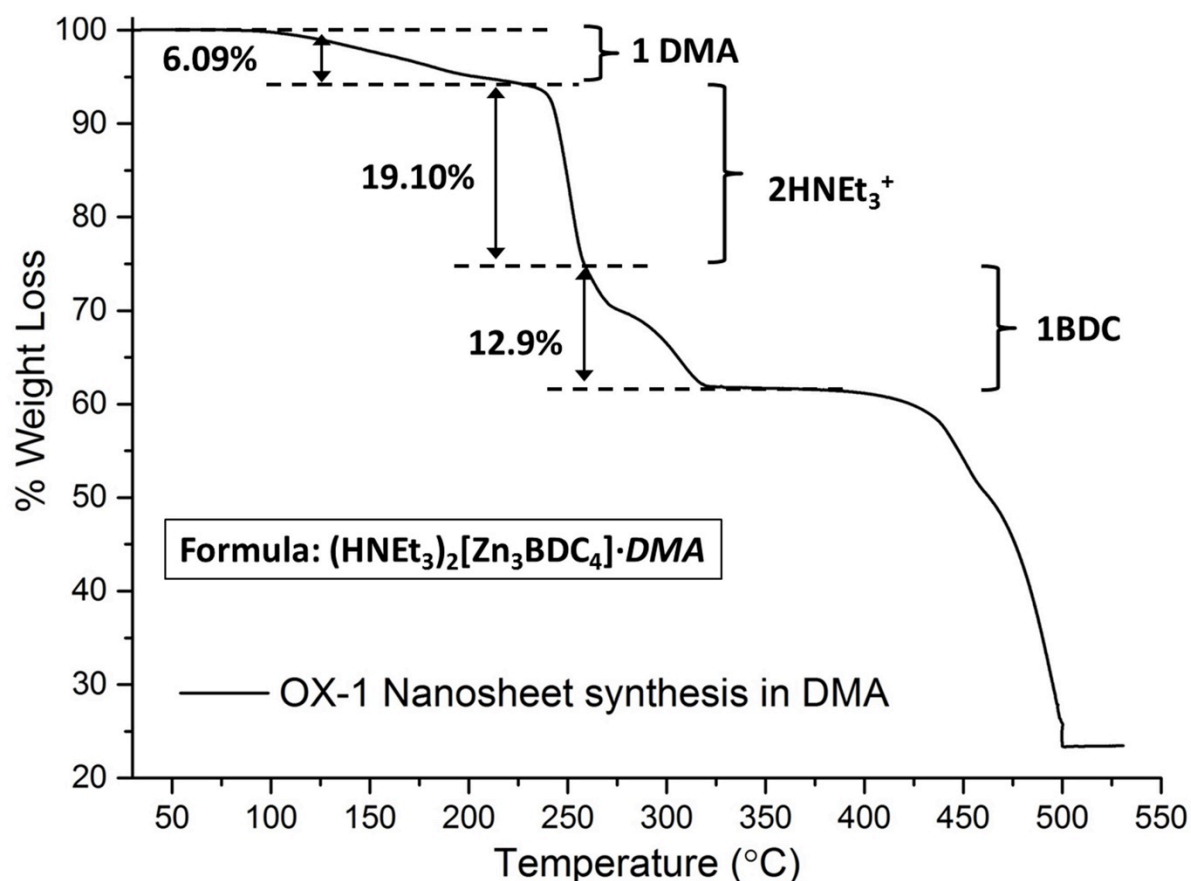


Figure S17. TGA for OX-1·DMA compound synthesized in N,N-Dimethylacetamide (DMA) with thorough washing and heat-vacuum treatment afterwards. Initial weight loss attributed to free solvent species that reveals entrapped solvent species cannot be removed by washing with low boiling solvent and heat-vacuum pre-treatments. (Washing step and pre-treatment conditions used were exactly the same for both compounds i.e. OX-1·DMF and OX-1·DMA, however, negligible initial weight loss for OX-1·DMF suggests removal of free solvents after pre-treatment. Conversely free solvents stay intact in OX-1·DMA even after pre-treatment).

8 Raman Spectroscopy

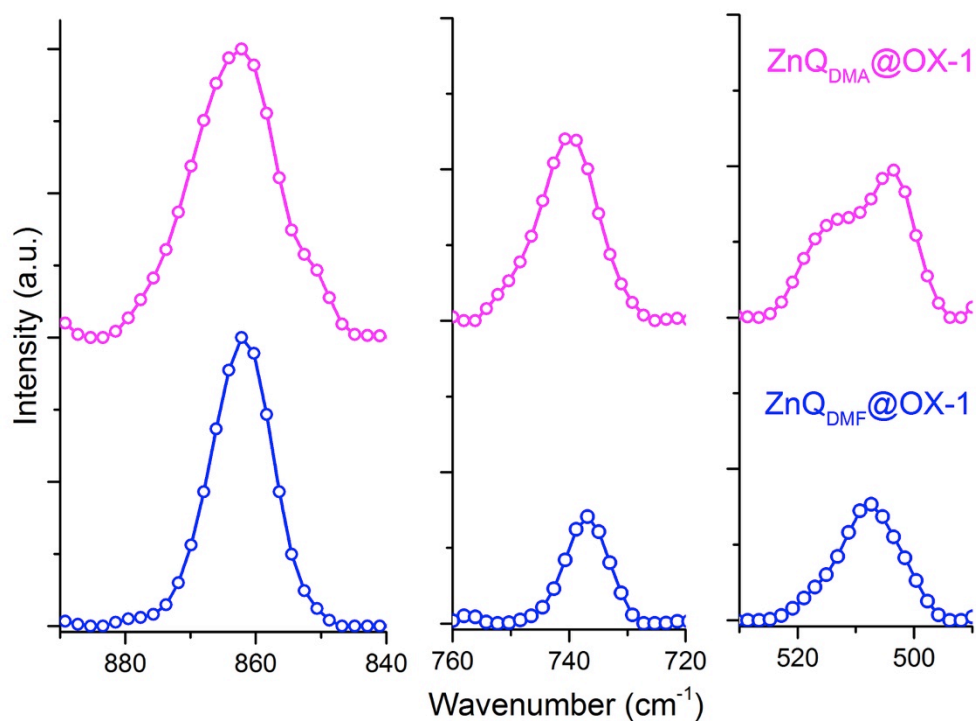


Figure S18. Raman modes of ZnQ_{DMF}@OX-1 and ZnQ_{DMA}@OX-1, the latter showing the doubly-degenerate bands at 852.2 cm⁻¹ and 514.04 cm⁻¹ arising from symmetry alterations of neat ZnQ guest emitter as affected by pore confinement. The full spectral range is given in main manuscript Fig. S2.

9 Quantum Yield and Lifetime of Pristine and Functionalized OX-1 Nanosheets

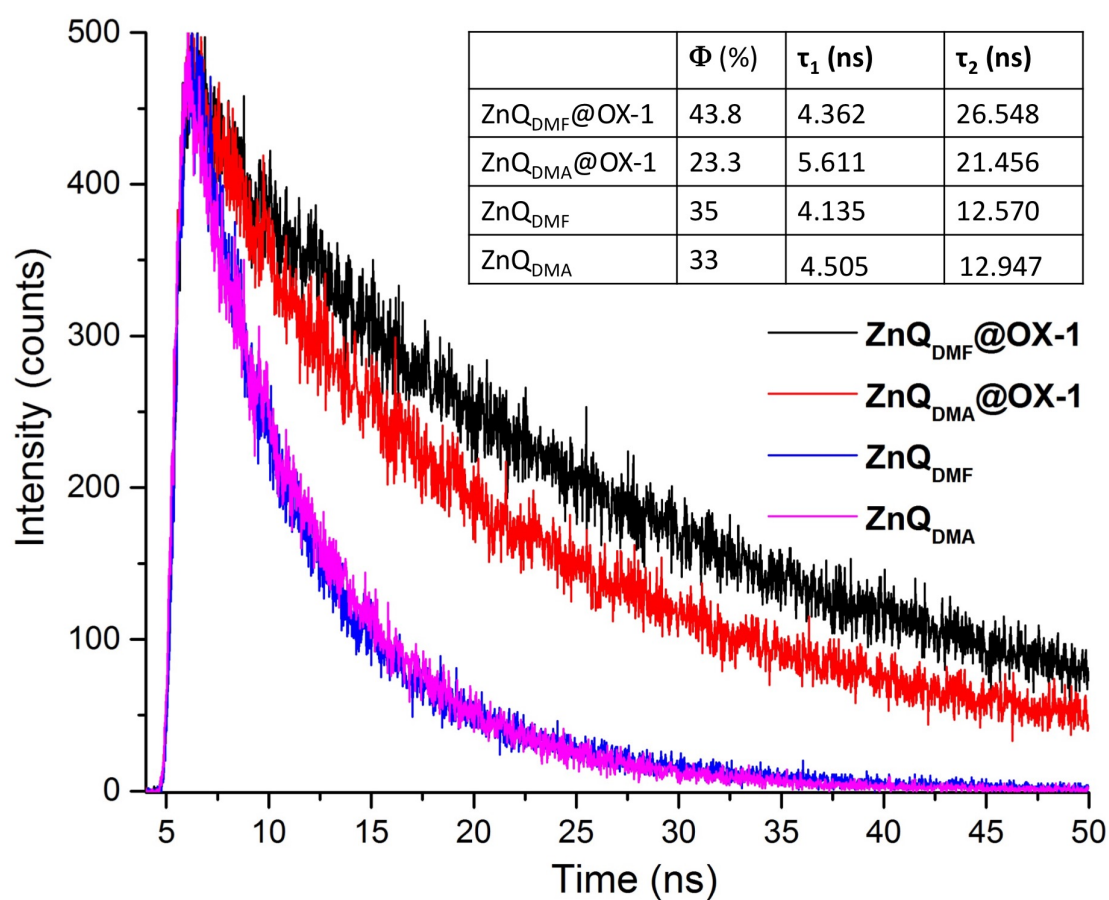


Figure S19. Fluorescence lifetime decay profiles for the (pure) ZnQ guest in DMF or DMA suspensions, and the Guest@OX-1 nanosheets revealing the nanoconfinement effects on the excited-state lifetime of fluorescent guest species. Φ is quantum yield (%) and τ are time constants (ns).

10 Geometry Optimization and Band Gap Calculations

Geometrical optimization was performed using the Forcite module implemented in Materials Studio v.8. For the OX-1 host framework structure, molecular cluster comprising a single pore was taken into consideration by using the 1×2×1 supercell, to calculate the plausible guest geometry as a result of host confinement effects.

Density functional theory (DFT) band gap calculations were performed using the DMol3 [4] module in Materials Studio v.8. We applied the generalized-gradient approximation (GGA) exchange-correlation functional by Perdew and Wang (PW91) [5] and the DNP basis set (double-numeric quality with polarization functions) [6]. Specific parameters used for HOMO-LUMO calculations of the host, guest, and guest@host assemblies are tabulated below:

```
ZnQDMF

# Task parameters
Calculate          energy
Symmetry           on
Max_memory         15000
File_usage         smart
Scf_density_convergence 1.000000e-006
Scf_charge_mixing  2.000000e-001
Scf_spin_mixing    5.000000e-001
Scf_diis           6 pulay
Scf_iterations     50

# Electronic parameters
Spin_polarization  unrestricted
Charge            0
Basis             dnp
Pseudopotential   none
Functional         gga(p91)
Aux_density       octupole
Integration_grid   fine
Occupation        fermi
Cutoff_Global     4.4000 angstrom
```

ZnQ_{DMA}

```
# Task parameters
Calculate          energy
Symmetry           on
Max_memory         15000
File_usage         smart
Scf_density_convergence 1.000000e-006
Scf_charge_mixing  2.000000e-001
Scf_spin_mixing    5.000000e-001
Scf_diis           6 pulay
Scf_iterations     50

# Electronic parameters
Spin_polarization  unrestricted
Charge             0
Basis              dnp
Pseudopotential   none
Functional         gga(p91)
Aux_density        octupole
Integration_grid   fine
Occupation         fermi
Cutoff_Global      4.4000 angstrom
```

ZnQ(Td)

```
# Task parameters
Calculate          energy
Symmetry           on
Max_memory         15000
File_usage         smart
Scf_density_convergence 1.000000e-006
Scf_charge_mixing  2.000000e-001
Scf_spin_mixing    5.000000e-001
Scf_diis           6 pulay
Scf_iterations     50

# Electronic parameters
Spin_polarization  unrestricted
Charge             0
Basis              dnp
Pseudopotential   none
Functional         gga(p91)
Aux_density        octupole
Integration_grid   fine
Occupation         fermi
Cutoff_Global      4.4000 angstrom
```

OX-1

```
# Electronic parameters
Spin_polarization    unrestricted
Charge              0
Basis               dnp
Pseudopotential     none
Functional           gga(p91)
Aux_density         octupole
Integration_grid     medium
Occupation          fermi
Cutoff_Global       4.4000 angstrom
Kpoints             off
```

ZnQ_{DMF}@OX-1

```
Symmetry            on
Max_memory          15000
File_usage          smart
Scf_density_convergence 1.000000e-006
Scf_charge_mixing   2.000000e-001
Scf_spin_mixing     5.000000e-001
Scf_diis            6 pulay
Scf_iterations      50
```

```
# Electronic parameters
Spin_polarization    unrestricted
Charge              0
Basis               dnp
Pseudopotential     none
Functional           gga(p91)
Aux_density         octupole
Integration_grid     medium
Occupation          fermi
Cutoff_Global       4.4000 angstrom
Kpoints             off
```

ZnQ(Td)@OX-1

```
Symmetry            on
Max_memory          15000
File_usage          smart
Scf_density_convergence 1.000000e-005
Scf_charge_mixing   2.000000e-001
Scf_spin_mixing     5.000000e-001
```

```
Scf_diis          6 pulay
Scf_iterations    50

# Electronic parameters
Spin_polarization  unrestricted
Charge            0
Basis             dnp
Pseudopotential   none
Functional         gga(p91)
Aux_density       octupole
Integration_grid   medium
Occupation        fermi
Cutoff_Global     3.9000 angstrom
Kpoints           off
```

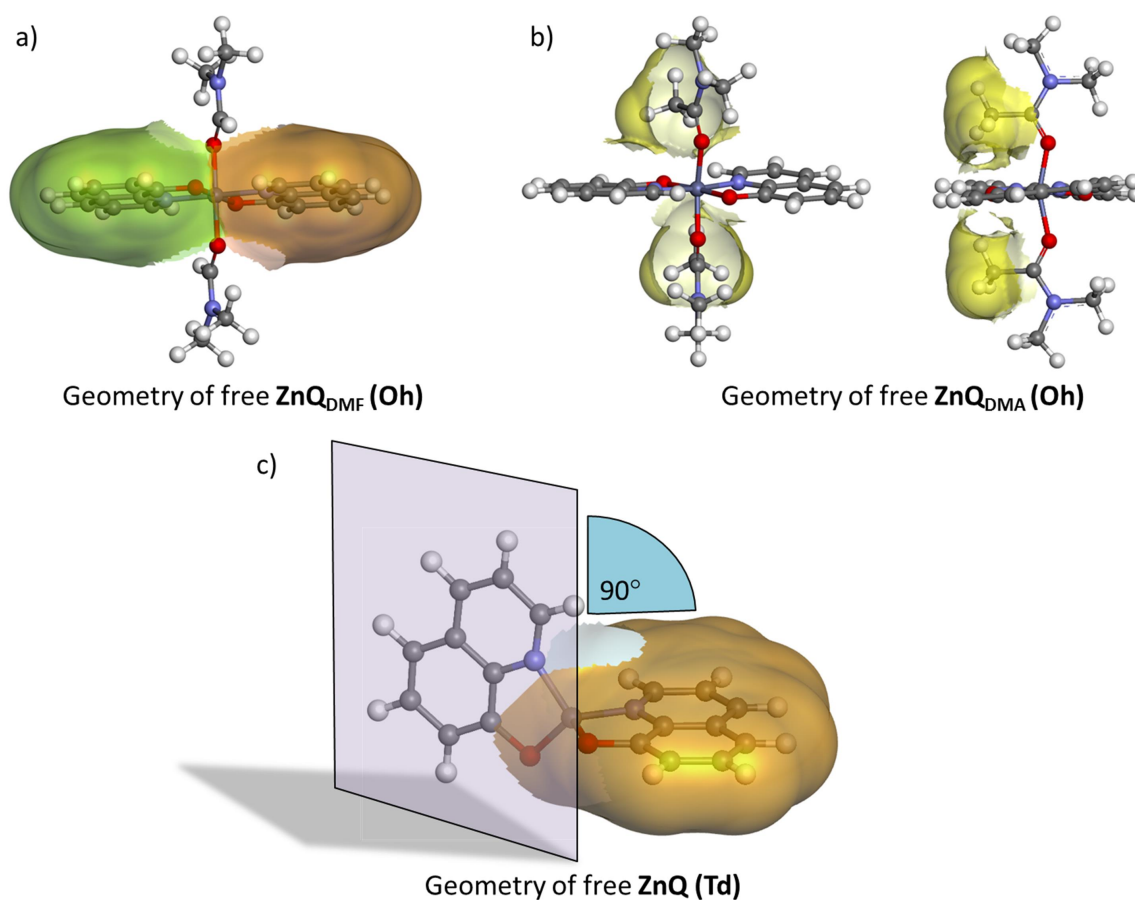


Figure S20. (a) Forcite optimized geometry of ZnQ_{DMF} showing coinciding planes of two 8-hydroxyquinoline molecules coordinated to the octahedral (Oh) Zn^{2+} centre, (b) ZnQ_{DMA} molecule from two different views shows the non-planarity of 8-hydroxyquinoline molecule due to bulkiness of CH_3 groups of the DMA molecule, (c) stable configuration of the ZnQ molecule in tetrahedral (Td) geometry of Zn^{2+} after removal of the two axially coordinated DMA solvent molecules.

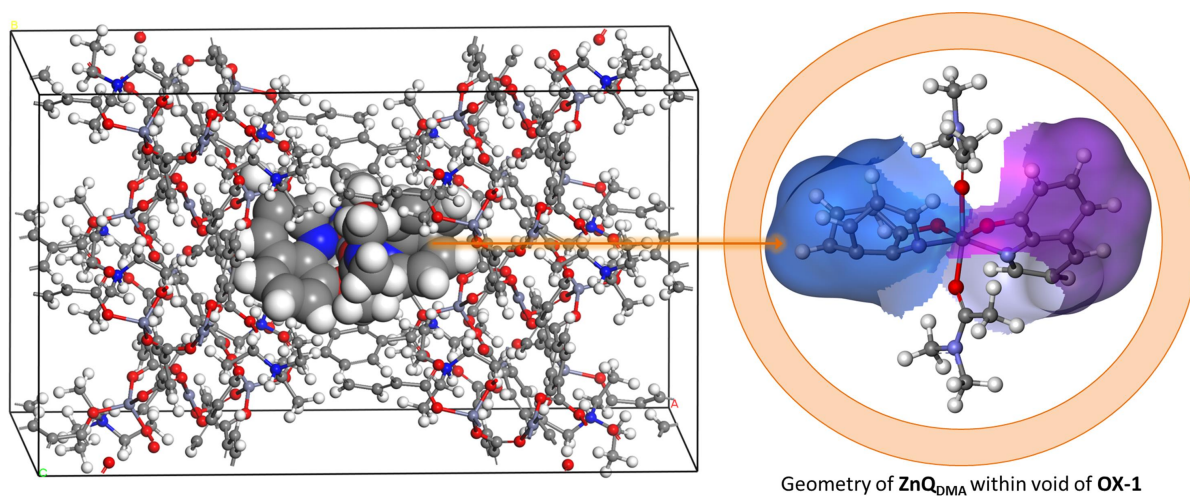


Figure S21. Extreme distortions of aromatic rings in ZnQ_{DMA} molecule in confined conditions of OX-1, suggesting unfavourable configuration for in-situ guest encapsulation and plausible removal of DMA molecules from the axial positions of Zn^{2+} centres during framework formation (in actual experiment).

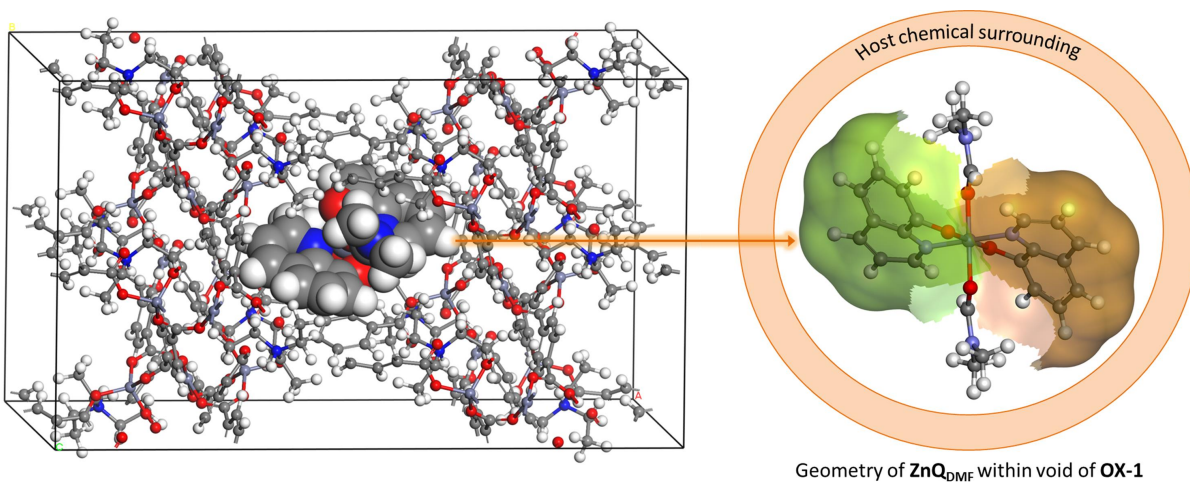


Figure S22. Optimised geometry of ZnQ_{DMF} molecule when constrained within the void of OX-1. Geometry was optimised using Forcite module in Materials Studio. Figure shows flipping of aromatic rings and slight distortion in the molecule due to confinement effects, which would cause modification in band gaps and resulting optical properties.

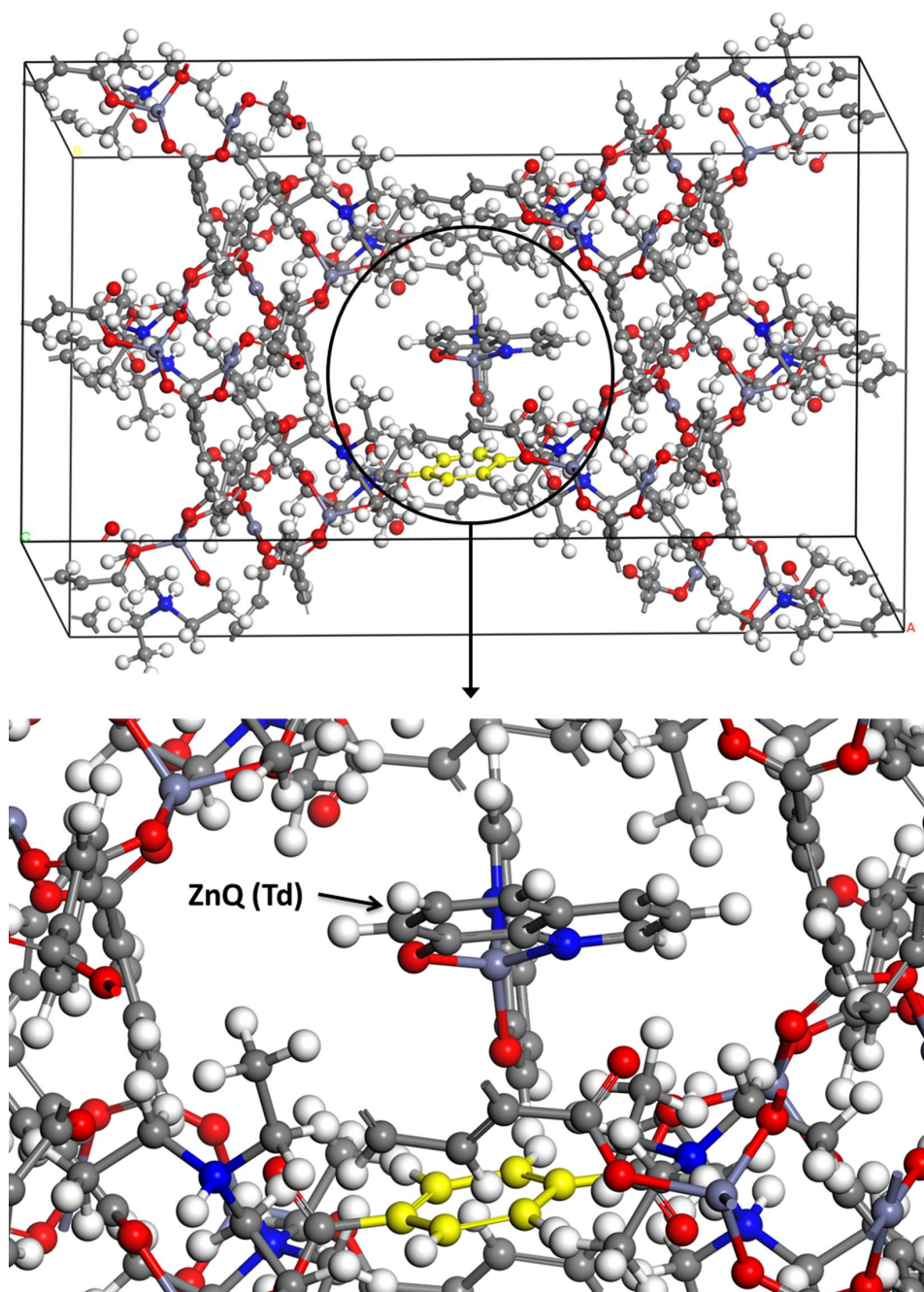


Figure S23. Stable geometry of ZnQ(Td) configuration (after removal of DMA molecules from the axial positions of Zn^{2+} centres) making weak interactions with the aromatic linkers of the OX-1 host. This host-guest configuration supports red shift in emission properties of $\text{ZnQ}_{\text{DMA}}@OX-1$ compound (Fig.2e) due to π - π interactions and H-bonding. Yellow highlighted ring represents an aromatic benzene ring from linker of host material.

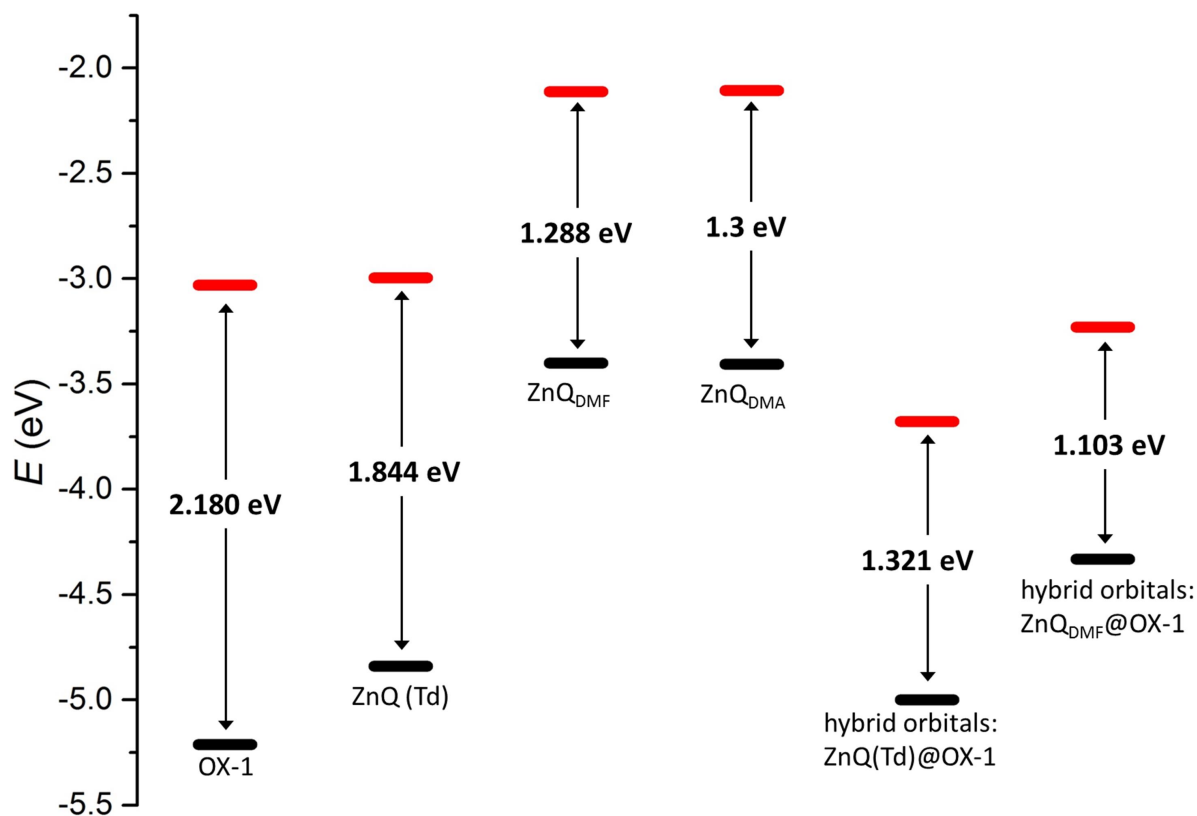
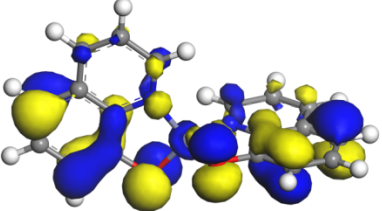
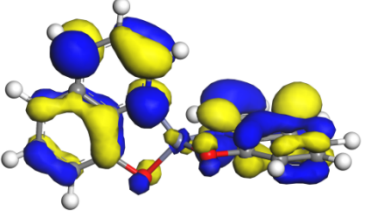
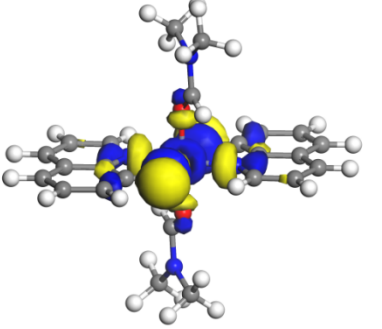
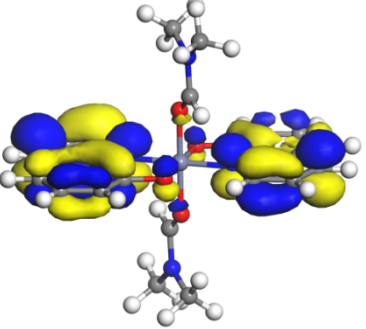
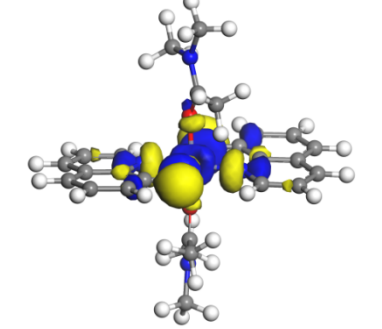
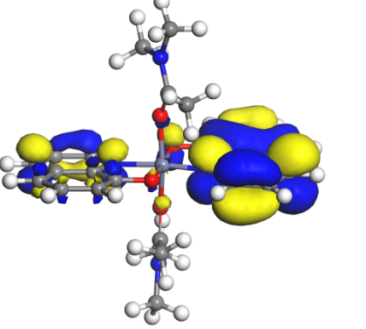
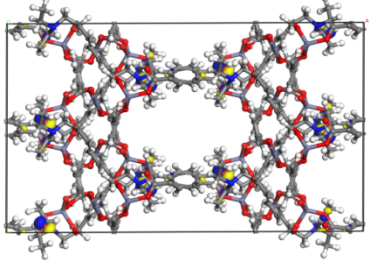
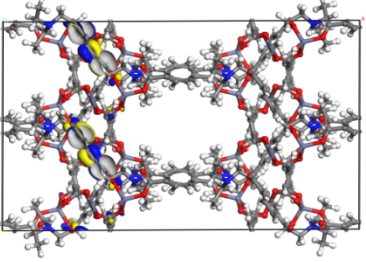
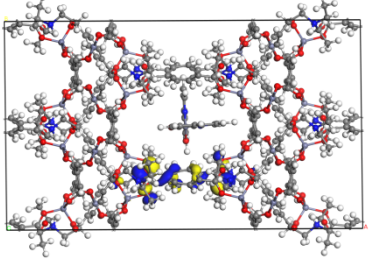
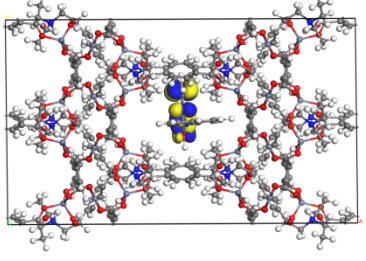
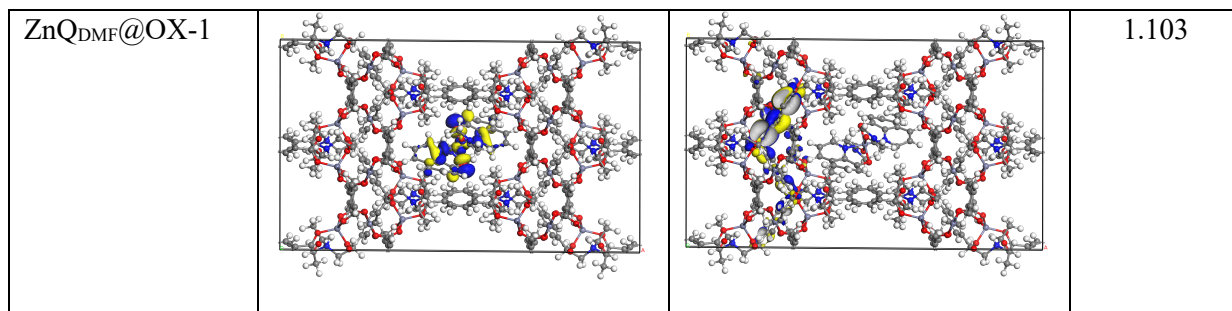


Figure S24. DFT calculated band gap energy values of the OX-1 host framework ($1 \times 2 \times 1$ supercell) and ZnQ guest emitter considering different possible host-guest configurations (DMF, DMA, Td). Formation of hybrid orbitals in Guest@OX-1 lowers the energy levels due to intimate host-guest interactions, shown on the right for the case of ZnQ(Td)@OX-1 and ZnQ_{DMF}@OX-1. Note that ZnQ_{DMA}@OX-1 is equivalent to ZnQ(Td)@OX-1, i.e. without DMA solvent coordination at its two axial positions (see Fig.S20b).

Table S2. HOMO and LUMO orbitals of different species involved in current work and their calculated band gap values (underestimation by DFT is well recognized [7] compared with experiments). Blue and yellow isosurfaces denote the positive and negative charges respectively.

Molecule	HOMO	LUMO	Band Gap (eV)
ZnQ (Td)			1.844
ZnQ _{DMF}			1.288
ZnQ _{DMA}			1.3
OX-1			2.180
ZnQ(Td)@OX-1 (equivalent to ZnQ _{DMA} @OX-1 obtained from DMA synthesis)			1.321



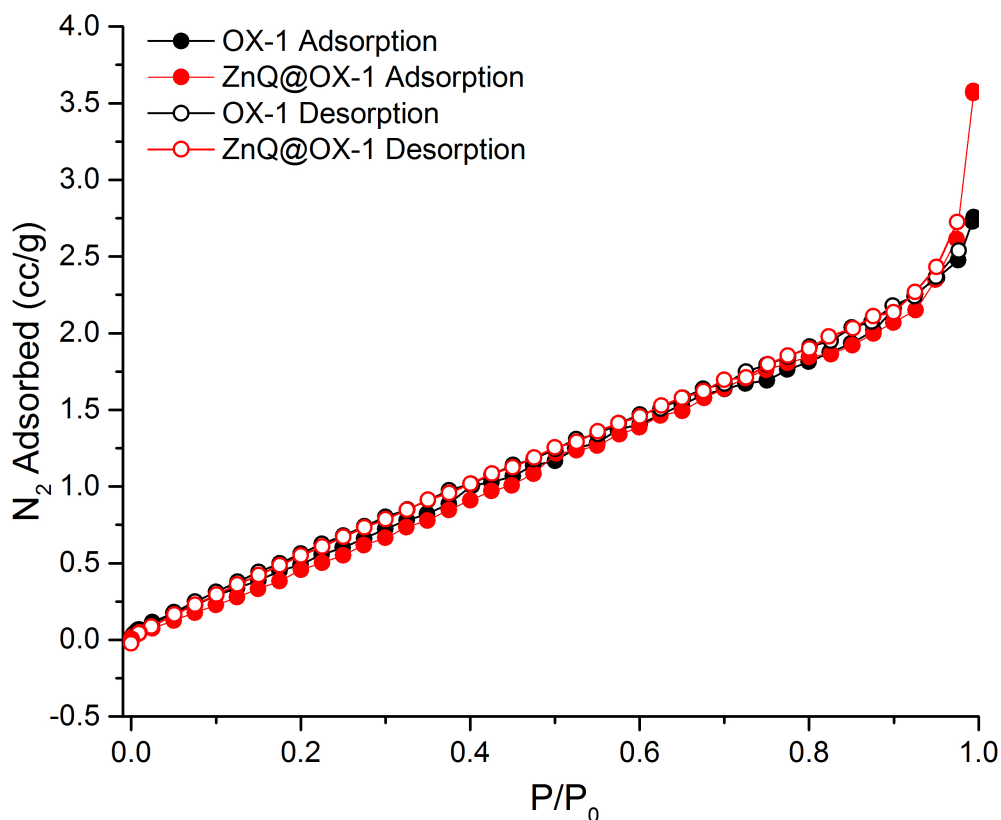


Figure S25. N_2 adsorption profile at 77 K for $ZnQ_{DMF}@OX-1$ and $OX-1$. Both samples were evacuated in the same way by heating at 80 °C under vacuum for 40 hr. Interestingly, we found that the isotherms of both compounds were similar, and with a relatively low BET surface area of $\sim 80 \text{ m}^2/\text{g}$. This value is reminiscent of the surface area of a similar framework structure ($(H_2NEt_2)_2[Zn_3(BDC)_4] \cdot 3DEF$, Langmuir surface $\sim 66 \text{ m}^2/\text{g}$) reported by Stock et al [2]. Negligible uptake suggests that $OX-1$ based nanosheets are non-reactive towards inert gas like N_2 , or there is also possibility of pore blockages due to restrictions in sample activation to remove entrapped species. Above notwithstanding, we note that $OX-1$ has a strong chemical affinity towards VOC analyte sensing (see Fig.S26-S27).

11 Host-Guest Interaction and Optochemical Stimulation

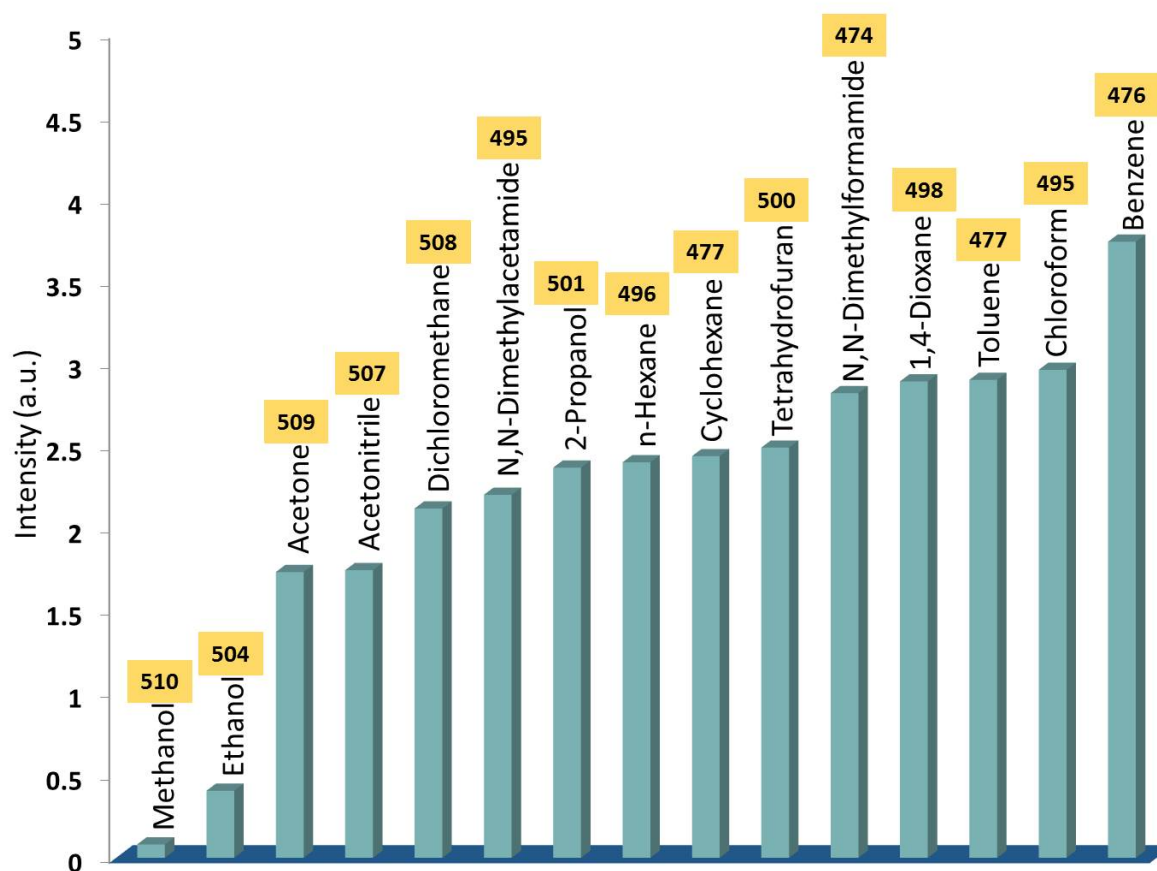


Figure S26. Small-molecule sensing ability of ZnQ_{DMF}@OX-1 nanosheets *via* changing emission intensity and shifting in wavelength due to optochemical perturbations in MOF pores. Numbers on top of each bar denotes the emission wavelength λ_{em} (nm).

Solvent analyte properties tabulated with the decreasing order of luminescence intensity of functionalized ZnQ_{DMF}@OX-1 material after analyte interaction. Solvent accessible surface area and volume are evaluated using Accelrys Discovery Studio Visualizer. α , β , and π^* are Kamlet-Taft [8] parameters describing ability of solvent to donate the proton, to accept the proton, and solvent dipolarity (polarizability), respectively.

No.	Solvent	Volume (Å ³)	Surface Area (Å ²)	β	α	π^*	λ_{em}
1	Benzene	80.11	100.793	0.1	0	0.59	476
2	Chloroform	72.684	93.789	0	0.44	0.58	495
3	Toluene	97.081	118.204	0.11	0	0.54	477
4	Dioxane	83.543	102.749	0.37	0	0.55	498
5	DMF	75.089	97.715	0.76	0	0.88	474
6	THF	73.885	93.672	0.55	0	0.58	500
7	Cyclohexane	98.279	114.683	0	0.001	0	477
8	n-Hexane	109.141	134.561	0	0	-0.08	496
9	2-Propanol	68.471	90.491	0.95	0.76	0.48	501
10	DMA	92.094	113.992	0.69	0	0.88	495
11	DCM	56.697	78.34	0	0.30	0.82	508
12	ACN	44.166	65.95	0.31	0.19	0.75	507
13	Acetone	62.921	85.788	0.48	0.08	0.71	509
14	Ethanol	51.117	73.915	0.77	0.83	0.54	504
15	Methanol	34.54	54.982	0.62	0.93	0.6	510

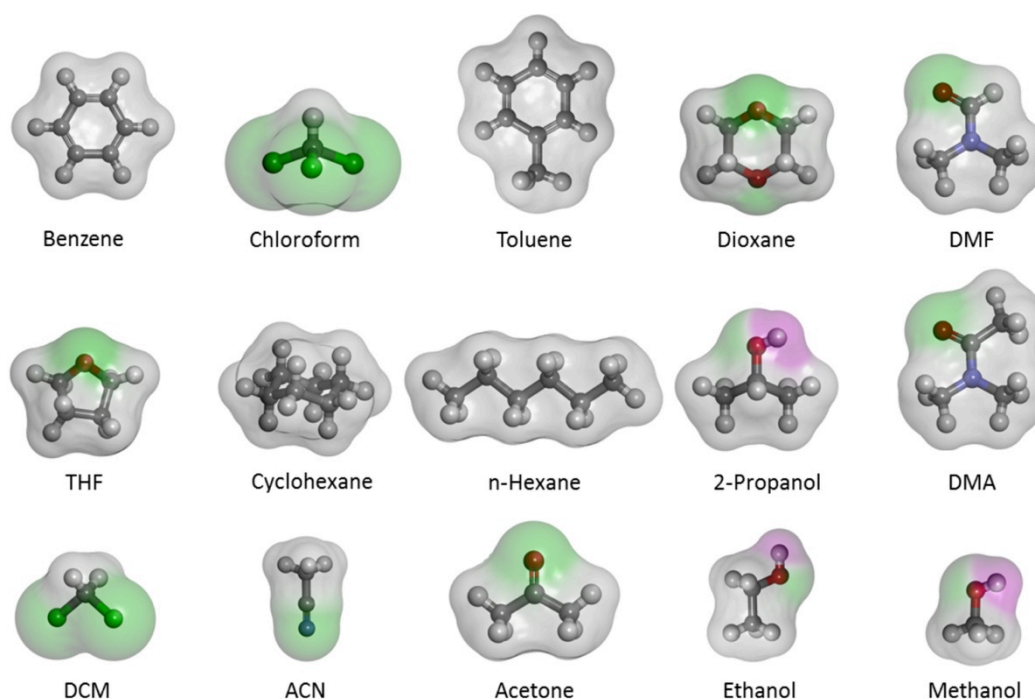



Figure S27. Hydrogen bond donor and acceptor surfaces of solvent analytes indicating hydrophobic sites in gray, hydrogen bond acceptor site in green, and hydrogen bond donor site in red color. Table above shows surface area and volume in numbers tabulated in the order of change in luminescence intensity.

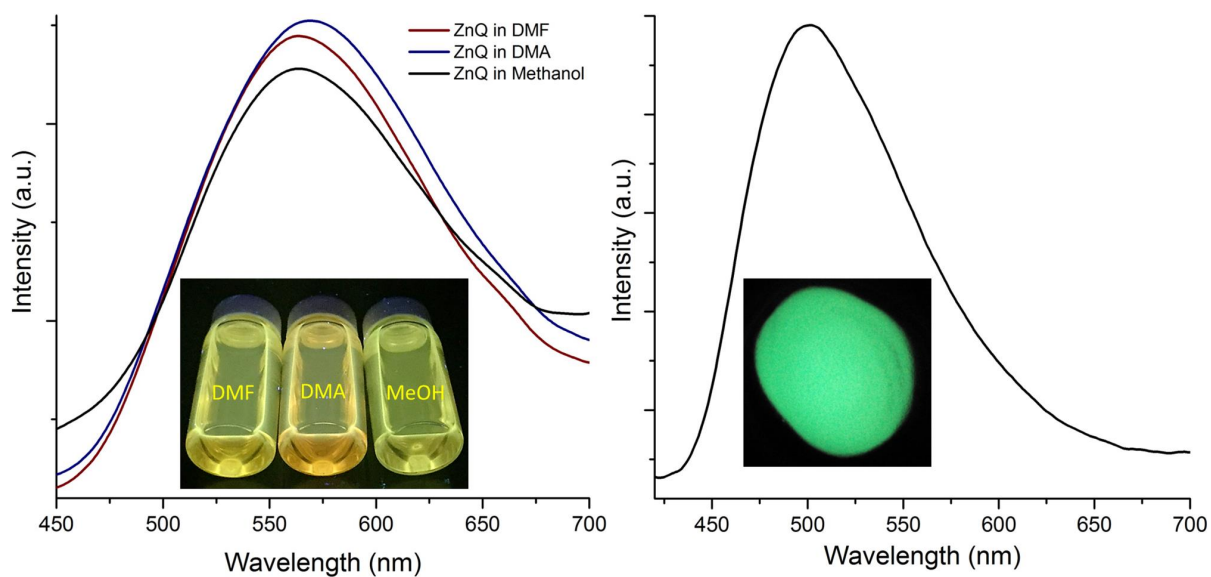


Figure S28. (a) Red-shifted emission spectra ($\lambda_{em} > 500$ nm) of pure ZnQ emitter complex dispersed in three different solvents: N,N-Dimethylformamide (DMF), N,N-Dimethylacetamide (DMA) and methanol. (b) Solid-state emission of pure ZnQ compound with $\lambda_{em} = 500$ nm. We studied emission behavior of the pure ZnQ complex in both liquid- and solid-states to achieve insights into the plausible molecular mechanism without nanoconfinement of MOF pores. In solid state (right), pure ZnQ emission is ~ 500 nm, however, when dispersed as solutions (left) in DMF, DMA or methanol, a red shift was observed at similar intensities. This result suggests intermolecular interaction is promoted in solution state due to its higher molecular mobility, originating from molecular overlapping to form strong aromatic π - π and H-bonding interactions, which are impeded in the solid state.

12 References

- [1] Burrows AD, Cassar K, Friend RMW, Mahon MF, Rigby SP, Warren JE. Solvent hydrolysis and templating effects in the synthesis of metal-organic frameworks, *CrystEngComm* 2005;7:548.
- [2] Biemmi E, Bein T, Stock N. Synthesis and characterization of a new metal organic framework structure with a 2D porous system: $(\text{H}_2\text{NEt}_2)_2[\text{Zn}_3(\text{BDC})_4]\cdot 3\text{DEF}$, *Solid State Sci.* 2006;8:363.
- [3] Macrae CF, Bruno IJ, Chisholm JA, Edgington PR, McCabe P, Pidcock E, Rodriguez-Monge L, Taylor R, van de Streek J, Wood PA. Mercury CSD 2.0 - new features for the visualization and investigation of crystal structures, *J. Appl. Crystallogr.* 2008;41:466.
- [4] Delley B. Time dependent density functional theory with DMol3, *J Phys Condens Matter* 2010;22:384208.
- [5] Patey MD, Dessent CEH. A PW91 Density Functional Study of Conformational Choice in 2-Phenylethanol, n-Butylbenzene, and Their Cations: Problems for Density Functional Theory?, *The Journal of Physical Chemistry A* 2002;106:4623.
- [6] Inada Y, Orita H. Efficiency of numerical basis sets for predicting the binding energies of hydrogen bonded complexes: evidence of small basis set superposition error compared to Gaussian basis sets, *J. Comput. Chem.* 2008;29:225.
- [7] Chan MK, Ceder G. Efficient band gap prediction for solids, *Phys. Rev. Lett.* 2010;105:196403.
- [8] Kamlet MJ, Abboud JLM, Abraham MH, Taft RW. Linear Solvation Energy Relationships .23. A Comprehensive Collection Of The Solvatochromic Parameters, Pi-Star, Alpha And Beta, And Some Methods For Simplifying The Generalized Solvatochromic Equation, *J. Org. Chem.* 1983;48:2877.